JBC RESEARCH ARTICLE

Degron-mediated proteolysis of CrhR-like DEAD-box RNA helicases in cyanobacteria

Received for publication, March 2, 2022, and in revised form, April 1, 2022 Published, Papers in Press, April 10, 2022,
https://doi.org/10.1016/j.jbc.2022.101925

Brendan T. Whitman[1], Cameron R. A. Murray[2], Denise S. Whitford[1], Simanta S. Paul[3], Richard P. Fahlman[2], Mark J. N. Glover[2], and George W. Owttrim[1,*]

From the [1]Department of Biological Sciences, [2]Department of Biochemistry, Faculty of Medicine & Dentistry, and [3]Department of Physics, University of Alberta, Edmonton, Alberta, Canada

Edited by Karin Musier-Forsyth

Conditional proteolytic degradation is an irreversible and highly regulated process that fulfills crucial regulatory functions in all organisms. As proteolytic targets tend to be critical metabolic or regulatory proteins, substrates are targeted for degradation only under appropriate conditions through the recognition of an amino acid sequence referred to as a "degron". DEAD-box RNA helicases mediate all aspects of RNA metabolism, contributing to cellular fitness. However, the mechanism by which abiotic-stress modulation of protein stability regulates bacterial helicase abundance has not been extensively characterized. Here, we provide *in vivo* evidence that proteolytic degradation of the cyanobacterial DEAD-box RNA helicase CrhR is conditional, being initiated by a temperature upshift from 20 to 30 °C in the model cyanobacterium, *Synechocystis* sp. PCC 6803. We show degradation requires a unique, highly conserved, inherently bipartite degron located in the C-terminal extension found only in CrhR-related RNA helicases in the phylum Cyanobacteria. However, although necessary, the degron is not sufficient for proteolysis, as disruption of RNA helicase activity and/or translation inhibits degradation. These results suggest a positive feedback mechanism involving a role for CrhR in expression of a crucial factor required for degradation. Furthermore, AlphaFold structural prediction indicated the C-terminal extension is a homodimerization domain with homology to other bacterial RNA helicases, and mass photometry data confirmed that CrhR exists as a dimer in solution at 22 °C. These structural data suggest a model wherein the CrhR degron is occluded at the dimerization interface but could be exposed if dimerization was disrupted by nonpermissive conditions.

Although energetically costly and irreversible, proteolytic degradation offers a rapid mechanism for adjusting the proteome under specific conditions when the continued presence of select proteins would be deleterious (1–3). Such conditional proteolytic pathways are catalyzed by ATP-dependent AAA+ proteases and represent a crucial component of post-translational regulation of gene expression in all organisms (4). For free living bacteria, AAA+ protease activity serves a critical role in cellular adaptation in response to the numerous and rapidly fluctuating conditions experienced in their natural environments. Accordingly, bacterial proteases contribute to the regulation of several crucial pathways including the cell cycle, induction of virulence, circadian clock synchronization, and biofilm formation (5–7). Recognition of specific protein targets in conditional proteolytic pathways is often achieved through amino acid motifs termed "degrons" that direct proteins to one or more bacterial AAA+ proteases under nonpermissive conditions (3). In the simplest scenario, bacterial degrons are necessary for direct binding to the protease; however, degrons may also bind adaptor proteins that mediate protease interaction (8).

A variety of degrons have been identified in bacteria including the ubiquitous N-degron pathway (9), the tmRNA ribosome rescue system (10), and a limited repertoire of relatively protein-specific degrons (11–15). Although proteomic and genetic approaches have expanded the catalog of bacterial proteins regulated by proteolytic degradation, the amino acid composition which constitute protein-specific degrons have rarely been experimentally verified. Detailed analysis of bacterial degrons has been hampered by their extended nature and general lack of conservation across bacteria, either in sequence or functionality (16–18). Similarly, the associated proteases frequently do not exhibit a high degree of degron or protein-class conservation (19–21). Degron sequences have been observed to vary considerably in the pathways targeted and also their length, composition, and location within a protein, indicating that our understanding of how protein degradation is regulated in bacteria is not complete. Examples illustrating bacterial degron diversity include an N-terminal 21 amino acid sequence containing a core region of hydrophobic residues surrounded by polar residues in the oxidative stress response regulator SoxS and, in contrast, a single histidine at the C terminus of the SOS response protein SulA required for targeting Lon-mediated turnover in *Escherichia coli* (22, 23).

Cyanobacteria are Gram-negative bacteria that constitute the only bacterial phylum that perform oxygenic photosynthesis, thereby representing a valuable platform for autotrophic production of bioproducts (24, 25). While evidence for N-degron–mediated degradation has been presented in cyanobacteria (26, 27), only three examples of sequence-specific

* For correspondence: George W. Owttrim, gowttrim@ualberta.ca.

degron-mediated proteolytic degradation have been reported. UmuD possesses a dual N-terminal degron consisting of an extended 19 amino acid sequence that targets proteolytic degradation by both N-degron and ClpX/P-associated pathways in *Synechocystis* sp. PCC 6803 (hereafter *Synechocystis*) (26). Second, the proteolytic adaptor NblA targets components of the light-harvesting phycobilisome complex during nitrogen starvation (28). Recently, the *Synechococcus elongatus* UTEX 2973 NblA was shown to bind a degron (F-D-A-F-T) at the N terminus of β-phycocyanin to initiate degradation (29). Finally, a C-terminal motif conserved in bacterial aldehyde decarbonylases, RMSAYGLAAA, governs degradation of *Prochlorococcus marinus* aldehyde decarbonylase in response to environmental stress (30). It can be deduced that degron-mediated proteolytic degradation likely plays a significantly expanded role in cyanobacteria, since they encode multiple protease duplications with nonoverlapping and essential physiological functions (31). However, these characteristics of the cyanobacterial proteolytic complement make it difficult to identify both degron sequences and the interacting proteases. Thus, identification of degron-regulation of posttranslational gene expression deserves further attention in cyanobacteria.

Previously, we reported that enhanced protein stability contributed significantly to the constantly elevated abundance of the cyanobacterial RNA helicase redox (CrhR), the only DEAD (Asp-Glu-Ala-Asp)-box RNA helicase encoded in *Synechocystis*, observed at low temperature (32). In response to the permissive abiotic stress, cold shock at 20 °C, *crhR* mRNA rapidly and transiently accumulates resulting in a 15-fold enhancement in CrhR protein abundance. Furthermore, CrhR continues to remain elevated at low temperature, despite the absence of *crhR* transcript, resulting from a significant increase in CrhR protein half-life. Repression of the low temperature induction was initiated by a temperature upshift to 30 °C resulting in conditional destabilization of CrhR and rapid degradation, leading to the basal levels observed at higher, nonpermissive temperatures (33). This study also showed that a truncated, biochemically inactive mutant of CrhR, $CrhR_{TR}$, was resistant to degradation during temperature upshift, suggesting an autoregulatory mechanism. While the degradation mechanism was not investigated further, the data suggested that either a targeting sequence necessary for proteolytic degradation had been deleted in $CrhR_{TR}$ and/or that CrhR RNA helicase activity was a requirement to activate the proteolysis machinery.

Physiologically, although initial transcript and proteomic analysis of WT, $crhR_{TR}$, and Δ*crhR* strains of *Synechocystis* have implicated CrhR in gene expression vital for supporting phototrophic metabolism, particularly at low temperatures, it remains unclear how dynamic regulation of CrhR at the posttranslational level is achieved or ultimately why it is necessary. The biochemical, genetic, and evolutionary principles governing control of CrhR abundance by the cell are therefore of prime interest in contextualizing RNA helicases within stress biology programming (34–36).

Here, we utilized an *in vivo* strategy to systematically identify a degron within the unique C-terminal extension (CTE) of CrhR that is essential for temperature upshift-mediated proteolytic degradation. Additionally, bioinformatics analysis indicated evolutionary conservation of the identified degron sequence in RNA helicases that are only encoded in the phylum Cyanobacteria. Proteolytic regulation of such "CrhR-type" RNA helicases may share a common mechanism and/or biological role, as they exhibited evolutionarily conserved temperature regulated induction and degradation kinetics in diverse cyanobacteria. Interestingly, although the CrhR degron sequence is necessary, it is not sufficient for proteolytic degradation as helicase function and *de novo* protein synthesis are also required. The results imply protease degradation of CrhR is autoregulatory through a positive feedback mechanism whereby CrhR enables translation of an unknown degradation factor(s). Induction and repression of proteolysis is also exquisitely sensitive to the magnitude of temperature shift, resulting in fine-tuning of CrhR abundance. Finally, mass photometry indicated CrhR exists as a dimer at 22 °C. AlphaFold 3D structural modeling predicted that the CTE is responsible for this dimerization behavior resulting in the degron being buried inside the interface, likely impeding recognition and degradation. Identification of this cyanobacterial-specific degron may provide a biotechnological tool to fine-tune posttranslational gene expression across multiple cyanobacterial genera.

Results

The CTE of CrhR-type RNA helicases contains an evolutionarily conserved temperature-responsive degron in cyanobacteria

It was of interest to determine if CrhR-related proteins were temperature regulated in other cyanobacteria. Alignment of the CrhR amino acid sequence downstream of the conserved HRIGR box indicated the presence of an ∼50 amino acid sequence spanning amino acids K386–W435 that was highly conserved in 22 orthologous helicases (Fig. 1*A*). The strength of this cross-species conservation is illustrated by the sequence logo generated from this region using Multiple Em for Motif Elicitation (MEME) software (Fig. 1*B*), produced using the cyanobacterial species listed in Table S1. Similar cold-induced accumulation combined with temperature upshift repression of CrhR-related RNA helicases was demonstrated in four representative cyanobacterial species (Fig. 1*C*). Note that the temperature shift response observed for CrhR in WT cells shown in Figure 1*C Synechocystis* exhibits a linear pattern of degradation, as observed previously (32). The kinetics of temperature downshift induced changes in CrhR-related protein abundance are presented in Figure 1*D*. Importantly, CrhR-like proteins in the four cyanobacterial species tested responded in a similar manner to temperature shift, increasing at 20 °C or 10 °C and decreasing at 30 °C. While the timelines and induction temperatures differed slightly between the four strains, the kinetics of induction and repression were consistent. The results suggest that an evolutionarily conserved, temperature responsive degradation motif is located in the CTE of CrhR-like cyanobacterial RNA helicases.

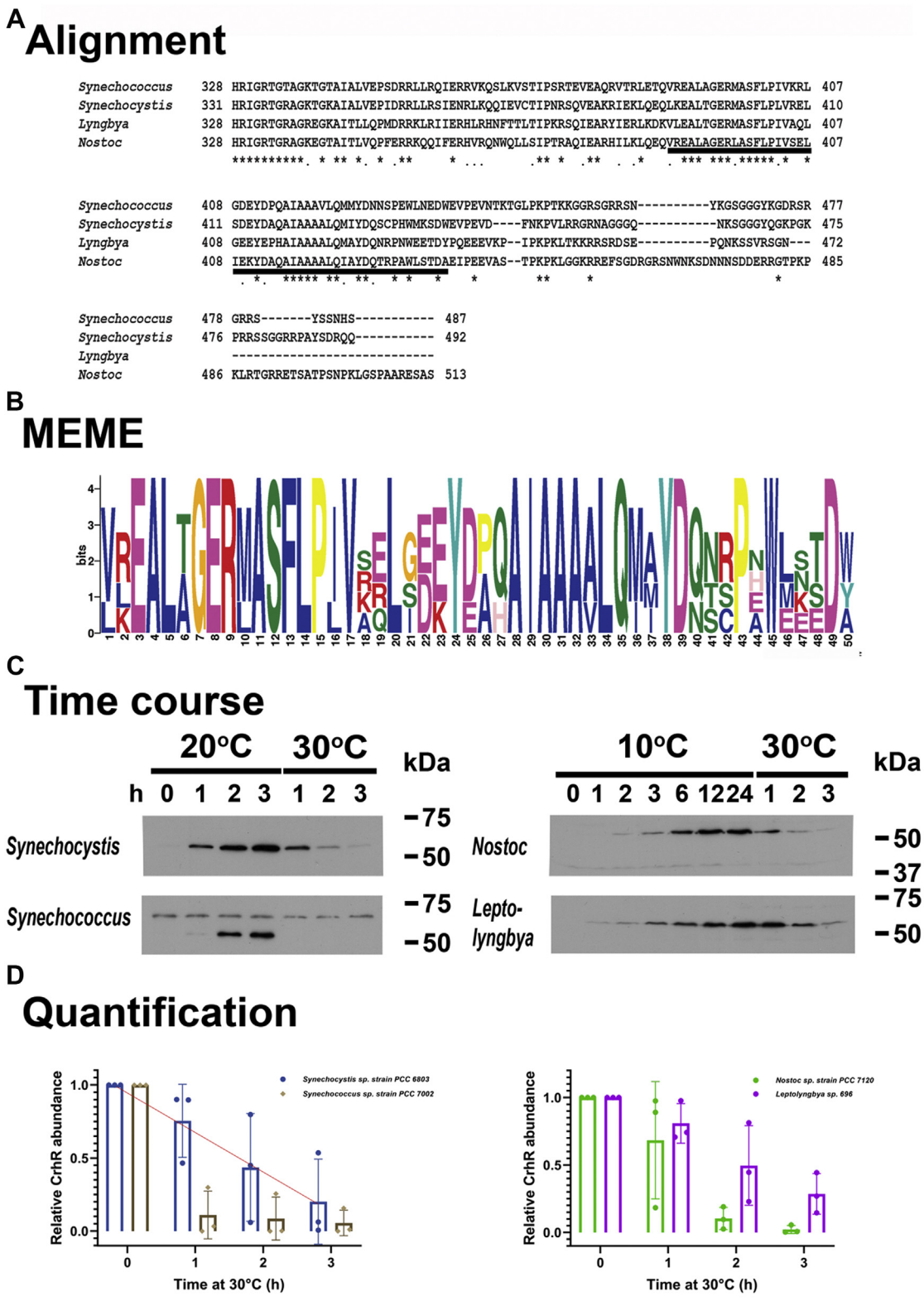

Figure 1. Cyanobacterial CrhR orthologs are temperature regulated and share a conserved C-terminal motif. *A*, residues constituting the CTE of four CrhR-like helicases from the indicated cyanobacteria were aligned using MUSCLE. The sequences were anchored by the helicase core HRIGR motif. Identical residues are marked by an *asterisk* and conserved residues by a period. The *Lyngbya aestuarii* RNA helicase, annotated as *deaD*, was substituted for *Lyngbya* sp. 696 based on close phylogenetic distance. *B*, an area of high CTE conservation representing the CrhR motif, as defined in this study, is visualized as a MEME logo using 25 RNA helicases orthologous to CrhR (71). Amino acid prevalence at each of the 50 sites is indicated by the bit score. *C*, cyanobacterial strains [*Synechocystis* (*Synechocystis* sp. PCC 6803); *Synechococcus* (*Synechococcus* sp. PCC 7002); *Nostoc* (*Nostoc* sp. PCC 7120); *Lyngbya* (*Leptolyngbya* sp. 696)] encoding a predicted CrhR-like helicase were subject to temperature shift to compare helicase degradation kinetics. Aliquots were harvested both during cold shock at either 20 °C (*Synechocystis*, *Synechococcus*) or 10 °C (*Lyngbya*, *Nostoc*), and after a return to 30 °C. Lanes contain either 10 μg of soluble protein extract (*Synechocystis*, *Synechococcus*) or 50 μg (*Lyngbya*, *Nostoc*). CrhR and CrhR-like helicases were detected using anti-CrhR antibody (1:5000) and visualized by ECL detection. *D*, quantification. Quantification of the relative abundance of the four CrhR-like polypeptides during induction and degradation

CrhR degradation depends on residues within the CTE

DEAD-box RNA helicases share a number of conserved motifs, including the characteristic DEAD motif, which comprise the highly conserved RNA helicase core (37) (Fig. 2*A*). N-terminal extension (NTE) and CTE provide specificity by facilitating protein–RNA and protein–protein interactions (38). To explore the possibility that a degron sequence within the CTE or NTE of CrhR is responsible for temperature upshift-mediated degradation, a series of deletions were generated in the *crhR* gene (Fig. 2*B*). Since deletion-induced alteration of protein folding could contribute to mutant polypeptide degradation or aggregation, we produced a diverse range of five N- or C-deletion constructions to examine. The most extensive C-terminal deletion, $CrhR_{\Delta R228\text{-}Q492}$, corresponds to the $CrhR_{TR}$ mutation, which produces a truncated polypeptide that can be detected readily in purified membrane and soluble *Synechocystis* cell lysis fractions (39), implying that even gross removal of the CTE does not produce instability or insoluble precipitates. Examination of temperature upshift induced degradation of the protein products expressed from the five constructs in WT *Synechocystis* indicated that an amino acid sequence between E393 and K449 was required for proteolytic degradation of the mutant protein (Fig. 2, *C–F*). This domain is located within the highly conserved C-terminal region identified in Figure 1, *A* and *B*.

Insightfully, the presence of mutant, nondegradable versions of CrhR did not affect degradation of WT CrhR nor did WT CrhR rescue degradation of mutated CrhR (Fig. 2, *C–F*). Again, a similar pattern of WT, genome-encoded CrhR degradation as shown in Figure 1*C Synechocystis* was observed, irrespective of the fate of the mutant form of CrhR present in each strain (Fig. 2, *C–F*).

Overall, the results shown in Figure 2, *C–F* and Fig. S1 provide crucial insights since they indicated that WT, biochemically active CrhR is required to activate degradation, but only of polypeptides that contain the degron. In addition, they demonstrate that plasmid-encoded CrhR polypeptides containing the degron are actively degraded, indicating analysis of the fate of CrhR polypeptides expressed from plasmids provide valid observations.

To better facilitate comparisons across strains or growth conditions, the linear nature of the decay curve for genome-encoded CrhR from *Synechocystis* (Fig. 1*D*) prompted us to assign linear degradation rates to all WT and mutant CrhR polypeptides. This analysis was performed by fitting linear regression models to abundance curves for either chromosomal expressed CrhR (Fig. S1*A*) or plasmid-encoded CrhR C-terminal deletions (Fig. S1*B*) in WT cells expressing functional CrhR. Linear regression models encompassing each time point from the entire 30 °C time courses during which degradation was occurring were found to closely correlate with abundance in all circumstances (Fig. S1*A*). Slopes of these regression lines, thus representing independent measurements of WT or mutant CrhR change in relative abundance over the entire time course, then enabled simultaneous visualization of pairwise comparisons in subsequent western analysis.

Examination of these degradation rate results indicated that the rate of change of chromosomal, WT CrhR does not vary appreciably in the presence of the CrhR-deletion constructs (Fig. 2*G* WT CrhR and Fig. S1*A*). In contrast, while degradation of the CrhRΔK449-Q492 mutant matched WT CrhR, abundance changes of the CrhRΔE393-Q492, CrhRΔA347-Q492, and the CrhRΔR228-Q492 deletion polypeptides varied significantly from the WT rate, indicating the degron motif had been deleted in these constructs (Fig. 2*G* Deletion CrhR constructs and Fig. S1*B*). Overall, the data indicated that the CrhR degron motif is located between E393 and K449 (Figs. 2, *C–G* and S1).

Delineation of a minimal core degron

A series of short, internal deletions were constructed within the 50 amino acid conserved region within the C-terminal motif to further delineate the location of the degron. Deletions in this region included 26 amino acids from the N terminus of this domain, $CrhR_{\Delta K386\text{-}S411}$, 24 amino acids from the C-terminal portion, $CrhR_{\Delta D412\text{-}W435}$, and the entire domain, $CrhR_{\Delta K386\text{-}W435}$. As a control, temperature-dependent CrhR accumulation in WT cells revealed the expected low temperature induction and subsequent temperature upshift repression (Fig. 3*A*), as observed in Figure 1*C Synechocystis*. Expression of the deletion constructs in WT cells indicated that while CrhR accumulation was relatively normal from the $CrhR_{\Delta K386\text{-}S411}$ construct (Fig. 3*B*), temperature regulation of the $CrhR_{\Delta D412\text{-}W435}$ (Fig. 3*C*) and $CrhR_{\Delta K386\text{-}W435}$ (Fig. 3*D*) constructs was significantly diminished.

Quantification of CrhR abundance changes in response to temperature upshift is provided in Figure 3*E*. As observed in Figures 1 and 2, *C–F*, the rate of change of genomic, WT CrhR did not vary appreciably in the presence of the fine CrhR-deletion constructs (Fig. 3*E* WT CrhR). In contrast, while degradation of the $CrhR_{\Delta K386\text{-}S411}$ polypeptide did not differ from the plasmid-encoded CrhR, abundance change trends of the $CrhR_{\Delta D412\text{-}W435}$ and $CrhR_{\Delta K386\text{-}W435}$ deletion polypeptides were abnormal, and degradation was significantly impaired (Fig. 3*E* mutant CrhR). These results suggested unequal contributions of the two segments of the 50 amino acid motif to CrhR regulation and that the $CrhR_{\Delta D412\text{-}W435}$ motif contains a sequence that, when absent, results in muted polypeptide turnover at 30 °C. Interestingly, the CrhR deletion mutants resistant to proteolytic degradation, $CrhR_{\Delta D412\text{-}W435}$ and $CrhR_{\Delta K386\text{-}W435}$, unexpectedly limited cold-induced induction of genomic-encoded CrhR at 20 °C but had no effect on temperature upshift degradation (Fig. 3, *B–D*).

was determined by measuring Western blot signals in *C* using Image Studio Lite (LI-COR Biosciences) software. Abundance ratios reflecting the relative intensity of CrhR at each time point as compared to the point of maximum induction at 30 °C (T = 0) were plotted. The *red line* in the *left panel* represents the linear regression of CrhR abundance in *Synechocystis* cells, indicating a constant rate of degradation. Results represent the average of three biological replicates, with error bars displaying the standard deviation (SD). CrhR, cyanobacterial RNA helicase redox; CTE, C-terminal extension.

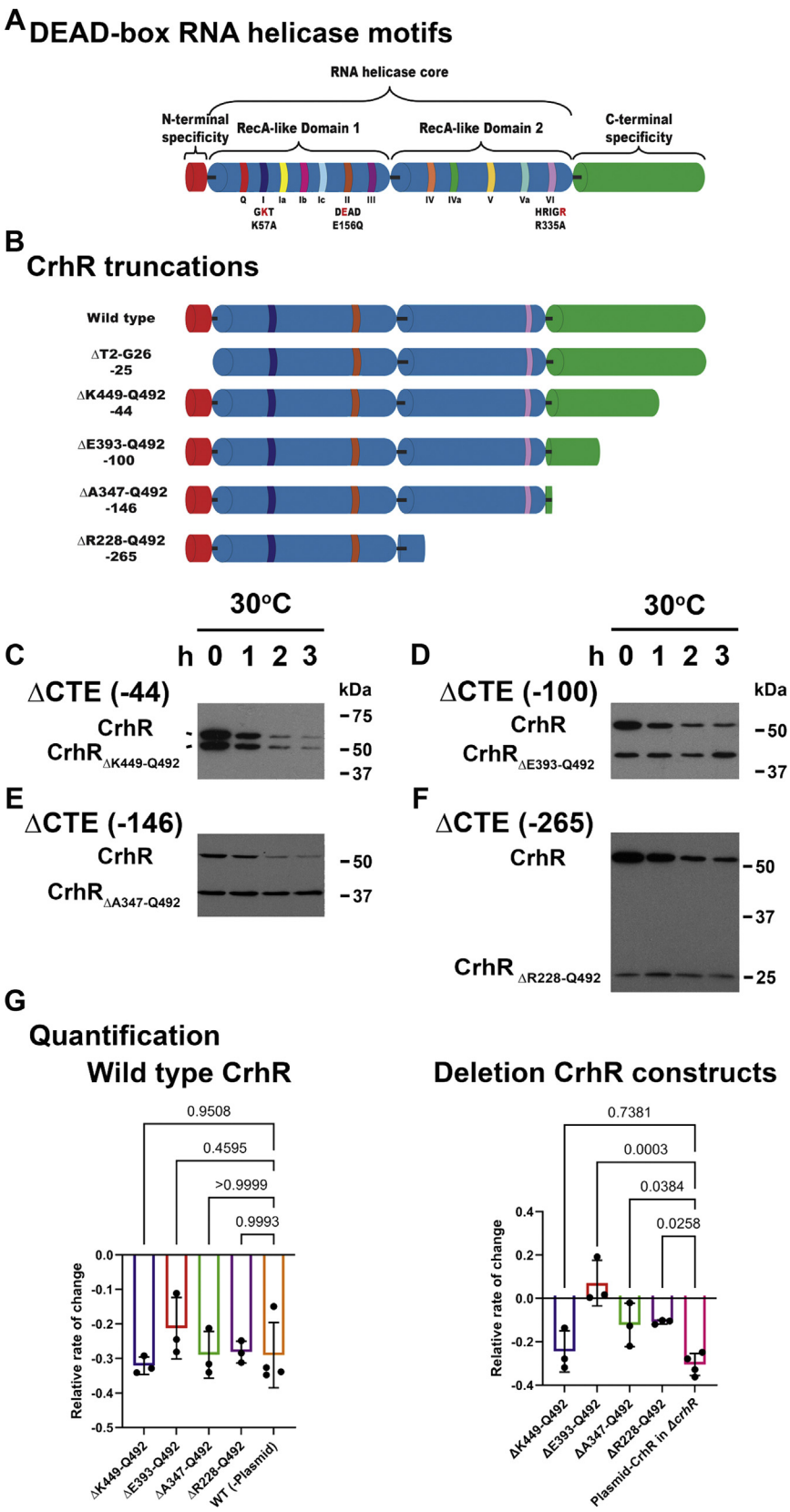

Figure 2. Residues in the C-terminal extension of CrhR enable temperature upshift-mediated degradation. *A*, structural depiction of conserved CrhR sequences. Conserved domains responsible for the biochemical activities of DEAD-box RNA helicases are labeled as per Linder and Jankowsky (37). Diagram drawn to scale. *B*, representation of the plasmid-encoded N- and C-deletion mutants used in this study. *C–F*, stability of the indicated truncated CrhR variants (CTE, C-terminal extension; -#, number of residues deleted from specified terminus) analyzed in WT *Synechocystis* during a temperature upshift from 20 to 30 °C. Samples were harvested at the indicated times after cells were cold shocked at 20 °C for 3 h to induce maximal CrhR accumulation (30 °C T = 0). Lanes contain 10 μg of soluble protein extract. *G*, quantification. Abundance ratios were derived as described in the Experimental procedures and Fig. S1

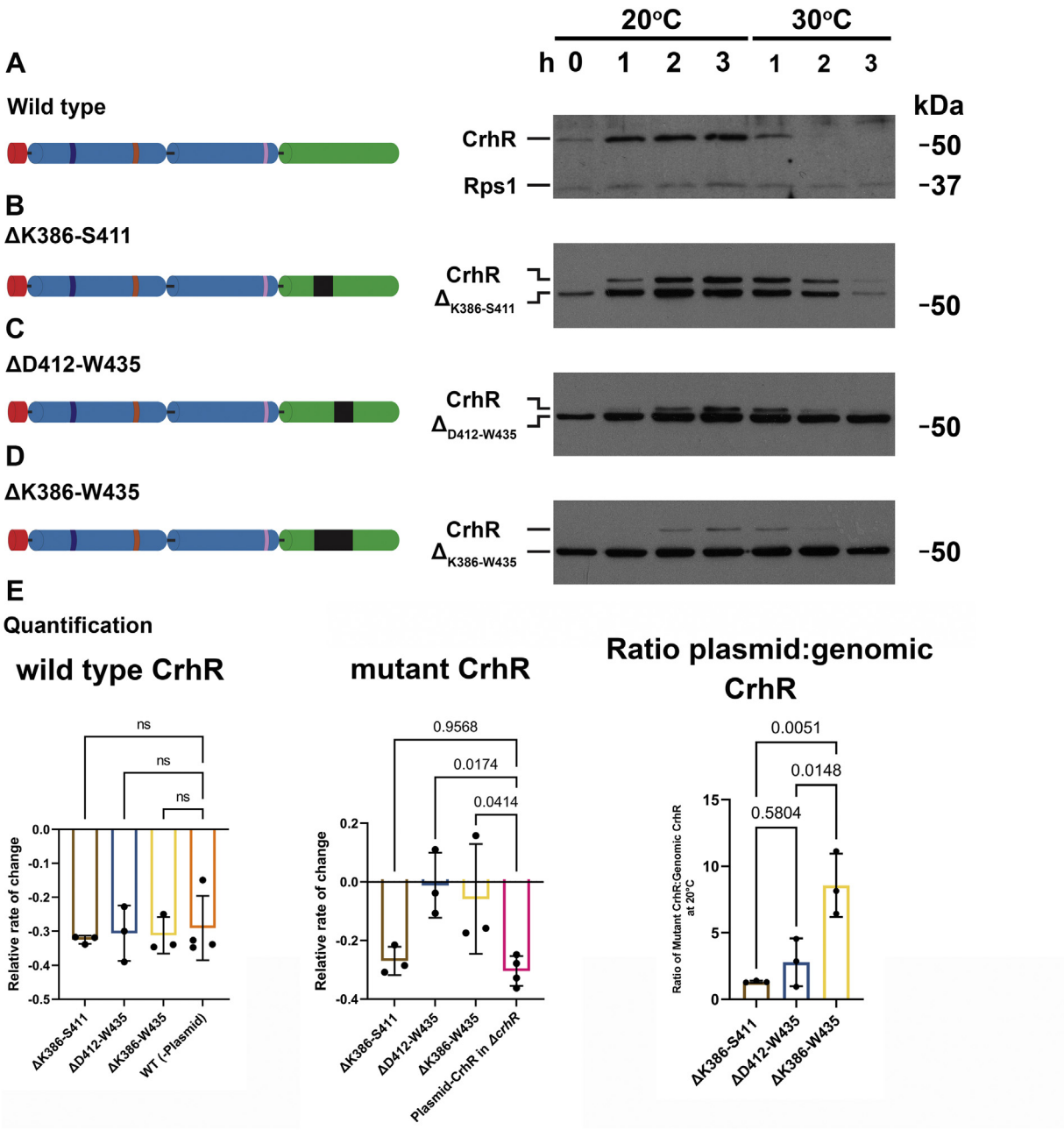

Figure 3. Internal deletions reveal the CrhR motif is comprised of two functional distinct domains. A schematic representation of the plasmid-encoded targeted deletions in the conserved 50 amino acid C-terminal motif is included adjacent to the corresponding western analysis. All analyses were performed in WT *Synechocystis* cells. *A*, WT. WT cells containing empty plasmid show normal 20 °C induction and 30 °C repression of CrhR. Rps1 was used as a protein loading control. *B–D*, abundance of deletion mutant polypeptides. Analysis of the effect of deletion of the indicated internal amino acid regions from the CrhR motif on abundance in WT cells. Expression of CrhR motif deletion mutants was characterized during induction at 20 °C and repression at 30 °C. Both WT 55 kDa CrhR and the deletion polypeptides expressed from a plasmid were detected. Lanes contain 25 μg of protein extract. Detection of CrhR and the deletion mutant polypeptides $CrhR_{\Delta K386\text{-}S411}$, $CrhR_{\Delta D412\text{-}W435}$, and $CrhR_{\Delta K386\text{-}W435}$ was performed by western analysis as described in Figure 2. *E*, quantification. Quantification graphs only depict degradation rates observed at 30 °C and not induction rates at 20 °C, for both chromosomal CrhR and mutant CrhR polypeptides. The ratio of plasmid-encoded CrhR to chromosomal-encoded CrhR polypeptides was quantified using signal from 20 °C T = 3 h extracts (Ratio plasmid:genomic CrhR) from Western blots performed on triplicate biological replicates. CrhR, cyanobacterial RNA helicase redox.

While deletion mutant suppression of WT CrhR accumulation was observed at all time points, we selected the point of maximum induction, 3 h at 20 °C, to quantitate the relative accumulation of plasmid-encoded mutant CrhR polypeptides to the abundance of the genomic-encoded WT polypeptide (Fig. 3*E* Ratio plasmid:genomic CrhR). As the functionality of

and converted into linear regression models by GraphPad Prism. Colored bars show the mean slope for each construct or control; error bars represent the SD. Significance values resulting from a Dunnett's multiple comparisons test to the control are given. Data were obtained from at least three biological replicates. The relative rate of change of WT CrhR (WT CrhR) abundance and deletion mutant polypeptides (Deletion mutant CrhR) are shown separately. CrhR, cyanobacterial RNA helicase redox.

the degradation domain decreased from $CrhR_{\Delta K386\text{-}S411}$ to $CrhR_{\Delta D412\text{-}W435}$ and $CrhR_{\Delta K386\text{-}W435}$, the ratio of mutant to WT CrhR increased significantly (Fig. 3*E* Ratio plasmid:genomic CrhR). Insightfully, this observation indicated that chromosomal CrhR abundance is proportionately reduced in response to the presence of increasing nondegradable CrhR. These results are the inverse of the stability seen for the respective mutations and suggested that the deletion polypeptides negatively feedback on WT, genome-encoded CrhR expression through an unknown mechanism. Overall, the results indicate that the primary degron motif was located between D412 and W435.

These intriguing observations prompted further examination of temperature regulation of the internal deletion constructs in a complete *crhR* deletion mutant, Δ*crhR*, to determine if proteolytic profiles differed in the absence of WT, genome-encoded RNA helicase activity. Similar to the pattern observed in Figure 1*C Synechocystis*, normal temperature-shift induction and repression were observed when the sole source of WT CrhR was expressed from a plasmid (Fig. 4*A*). In comparison to degradation observed in Figure 1*C Synechocystis* and Figure 2, *C–F*, for WT, genome-encoded CrhR, while essentially identical temperature regulation was observed for the $CrhR_{\Delta K386\text{-}S411}$ mutant (Fig. 4*B*), both temperature downshift and upshift induction and repression of the system were absent in the $CrhR_{\Delta D412\text{-}W435}$ (Fig. 4*C*) and $CrhR_{\Delta K386\text{-}W435}$ (Fig. 4*D*) strains. Given the high degree of conservation and location within the essential C-terminal portion of the CrhR motif, a further deletion encompassing the region between Q_{417} and Q_{425} ($CrhR_{\Delta Q417\text{-}Q425}$) was generated in an attempt to define a minimal degron. The importance of the Q417-Q425 region for the functional degron was emphasized by the partial loss of temperature regulation (Fig. 4*E*). The NTE was not significantly associated with degradation since absence of the $NTE_{2–26}$ had no effect on induction or repression in Δ*crhR* cells (Fig. 4*F*). Quantification indicated that while the $CrhR_{\Delta K386\text{-}S411}$ and $NTE_{2–26}$ polypeptides degraded at a rate similar to WT CrhR, the rate of $CrhR_{\Delta Q417\text{-}Q425}$ degradation was intermediate and $CrhR_{\Delta D412\text{-}W435}$ and $CrhR_{\Delta K386\text{-}W435}$ degraded at a significantly reduced rate (Fig. 4*G*).

Taken together, the data indicated the presence of an extended degron within the CrhR CTE, $CrhR_{\Delta D412\text{-}W435}$, with residues spanning Q_{417} and Q_{425} specifically performing a major role in the degradation mechanism.

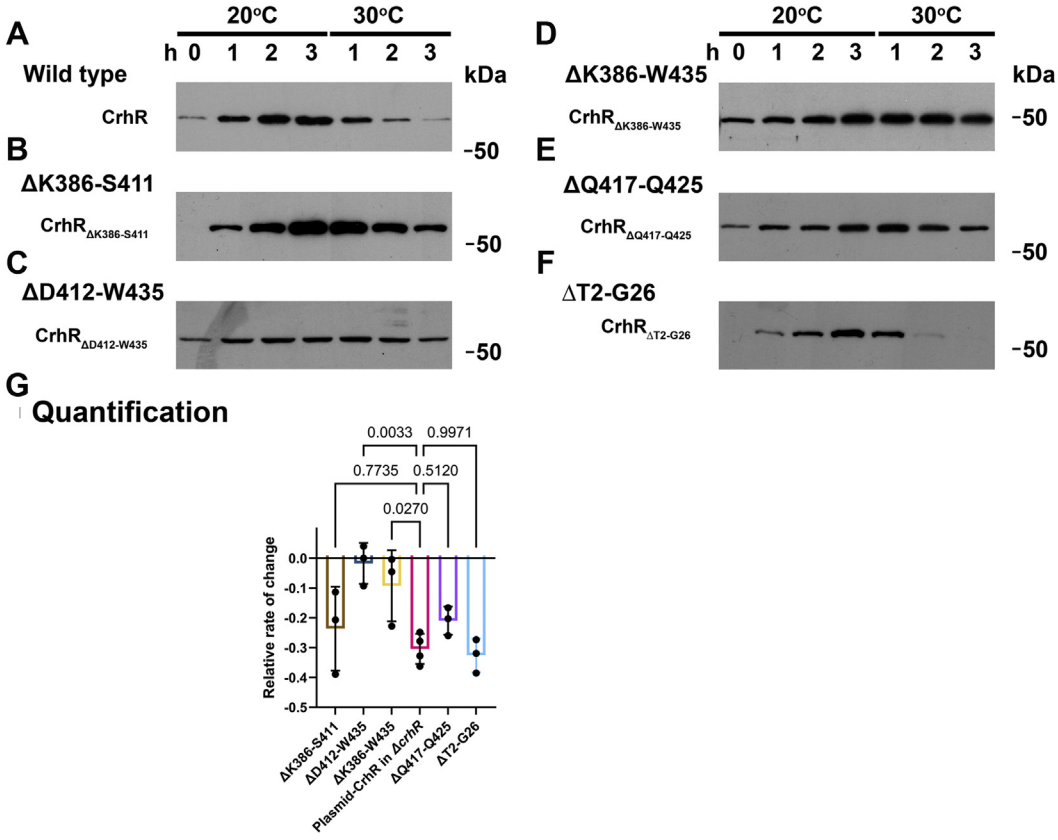

Figure 4. The CrhR motif influences stability during temperature shift in the absence of CrhR RNA helicase activity. All analyses were performed in the complete *crhR* ORF mutant, Δ*crhR*, in the absence of WT CrhR RNA helicase activity in response to temperature downshift and upshift. *A*, Δ*crhR*. WT CrhR was expressed in Δ*crhR* cells from the B1 plasmid containing the complete native promoter and *crhR* ORF. *B–D*, expression profiles of the indicated plasmid-encoded motif deletion mutants in Δ*crhR*. *E*, minimal degron. A finer deletion, encompassing Q417 to Q425, a region within the $CrhR_{\Delta D412\text{-}W435}$ portion of the CrhR motif, was characterized in relation to previous motif deletions. *F*, N-terminal deletion. Expression of the $CrhR_{\Delta T2\text{-}G26}$ N-terminal deletion mutant was analyzed in the Δ*crhR* strain. Lanes contain 15 μg of protein extract. $CrhR_{\Delta Q417\text{-}Q425}$, $CrhR_{\Delta T2\text{-}G26}$, and the motif mutants shown in Figure 3*A* were detected by Western blotting as described in Figure 1. *G*, quantification. Quantification was only performed to evaluate degradation rates observed at 30 °C, and not induction rates at 20 °C, for the indicated CrhR polypeptides, as described in Figure 2. CrhR, cyanobacterial RNA helicase redox.

RNA helicase activity is required for degradation

We then asked if CrhR RNA helicase activity was required to initiate a robust proteolytic response. The location of three point mutations, K57A (Walker ATPase box A), E156Q (DEAD box II), or R335A (HRIGR box VI), known to inhibit RNA helicase biochemical activity (40–42) are depicted in Figures 2, *A* and *B* and 5*A*. Addition of an N-terminal 6X-His tag was utilized to differentiate the biochemical mutants from full-length CrhR in WT cells. Fusion of an N-terminal 6X-His tag is known to have no discernable effect on CrhR RNA helicase activity (43). None of the biochemical mutants affected temperature induction or repression of either mutant or WT CrhR expression in WT cells expressing native, functionally active CrhR (Fig. 5*B*). In sharp contrast, all three biochemical mutants abolished both induction and repression in Δ*crhR* cells (Fig. 5*C*). These results suggest an autoregulatory mechanism whereby RNA helicase activity is a corequisite for degradation in addition to the presence of the degron. Separate quantification of the abundance of WT, genome-encoded CrhR and the plasmid-expressed 6X-His-CrhR point mutants is shown in Figure 5*D*. As shown in analysis presented above, WT CrhR abundance was again not altered in the presence of the CrhR point mutant polypeptides (Fig. 5*D* WT CrhR). Similarly, abundance of the point mutants decreased in the presence of WT CrhR although at a slower rate (Fig. 5*D* MT CrhR). In comparison, temperature shift induction and repression of the three-point mutants was abolished in the absence of WT CrhR (Fig. 5*D* Δ*crhR* cells MT CrhR).

CrhR repression can be activated by removal of CrhR inducing abiotic stresses

Previous evidence from our lab indicated that CrhR induction occurs in response to a variety of abiotic stresses that regulate induction *via* a common effect on the redox potential of the electron transport chain, independent of temperature shift (44). As a result, it was of interest to determine if temperature-independent degradation of CrhR, similar to that observed during temperature upshift, occurred in response to removal of these abiotic stresses. CrhR abundance was assessed following removal of NaCl and sorbitol stress at 30 °C, in the absence of low temperature stress (Fig. 6).

A similar rate of degradation as that observed in control WT cells expressing genome encoded in response to a 20 to 30 °C upshift (Fig. 6*A*) was observed upon removal of both NaCl and sorbitol stress in the absence of temperature stress (Fig. 6*B* NaCl and Fig. 6*C* sorbitol), as quantified in Figure 6*D* Quantification. Overall, the results agree with and extend previous work suggesting that the sensor for CrhR turnover can respond to a range of abiotic stress conditions in addition to temperature fluctuation.

CrhR proteolysis is adaptive and relies on sustained translation elongation

We have previously shown that antibiotics blocking either translation initiation or elongation have divergent effects on the *in vivo* degradation of CrhR (33). Here, it was explored whether translational interference could influence proteolytic degradation once cold shocked cells had already initiated degradation in response to an upshift to 30 °C (Fig. 7). First, in the absence of antibiotics, the expected pattern of rapid temperature-downshift induction and temperature-upshift induced degradation was observed (Fig. 7*A*). Based on the decrease in CrhR abundance after 30 min observed in Figure 7*A*, translational inhibitors were added at this time point for all subsequent treatments. Looking initially at the temperature upshift effects under these conditions, it was observed that further degradation of CrhR could be effectively blocked by chloramphenicol but not by kanamycin treatment (compare Fig. 7, *A*–*C*). Therefore, continued translation elongation but not initiation was essential for maintaining CrhR degradation. Furthermore, addition of the transcriptional inhibitor rifampicin failed to prevent CrhR turnover, signifying *de novo* transcription is not required to maintain proteolysis but was required for subsequent temperature downshift induction (Fig. 7*D*). These interpretations were confirmed by quantification of the relative rate of degradation that indicated a similar rate to WT CrhR in cells treated with kanamycin and rifampicin, but a rate that was significantly reduced in chloramphenicol-treated cells (Fig. 7*E*).

These cultures were also used to extend this analysis where the interplay between CrhR degradation and induction was examined for translational inhibitor treated and untreated cells in response to subsequent temperature downshift to 20 °C. Interestingly, proteolysis was rapidly reversed in response to temperature downshift in control cells in the absence of inhibitors with normal CrhR induction recovering within 15 min after temperature downshift to 20 °C (Fig. 7*A*). Kanamycin permitted a minimal level of low temperature induction, suggesting protein synthesis was incompletely blocked at the inhibitor concentration used (Fig. 7*B*), indicating that translation was not completely inactivated. In contrast, chloramphenicol and rifampicin abolished low temperature induction (Fig. 7, *C* and *D*). The rate of decline in rifampicin matches the degradation rate observed in WT cells at 30 °C (Fig. 7*E*). This illustrates that *de novo* transcription and proteolysis act in concert to produce growth condition appropriate levels of CrhR.

These observations crucially indicated that proteolytic degradation was not an all or none process and is susceptible to rapid inactivation at the permissive temperature, 20 °C. Overall, CrhR degradation is a dynamic process contingent on continued transcription and protein synthesis coordinated by a signal propagated by incubation at the higher, nonpermissive temperature.

The rate of CrhR degradation is temperature dependent

Further insights into the temperature dependence of CrhR proteolysis were obtained by determining the rate of degradation in response to increasing magnitude of temperature upshift as shown in Figure 8. Although CrhR performs a vital physiological role in the cell at 20 °C, CrhR also functions at

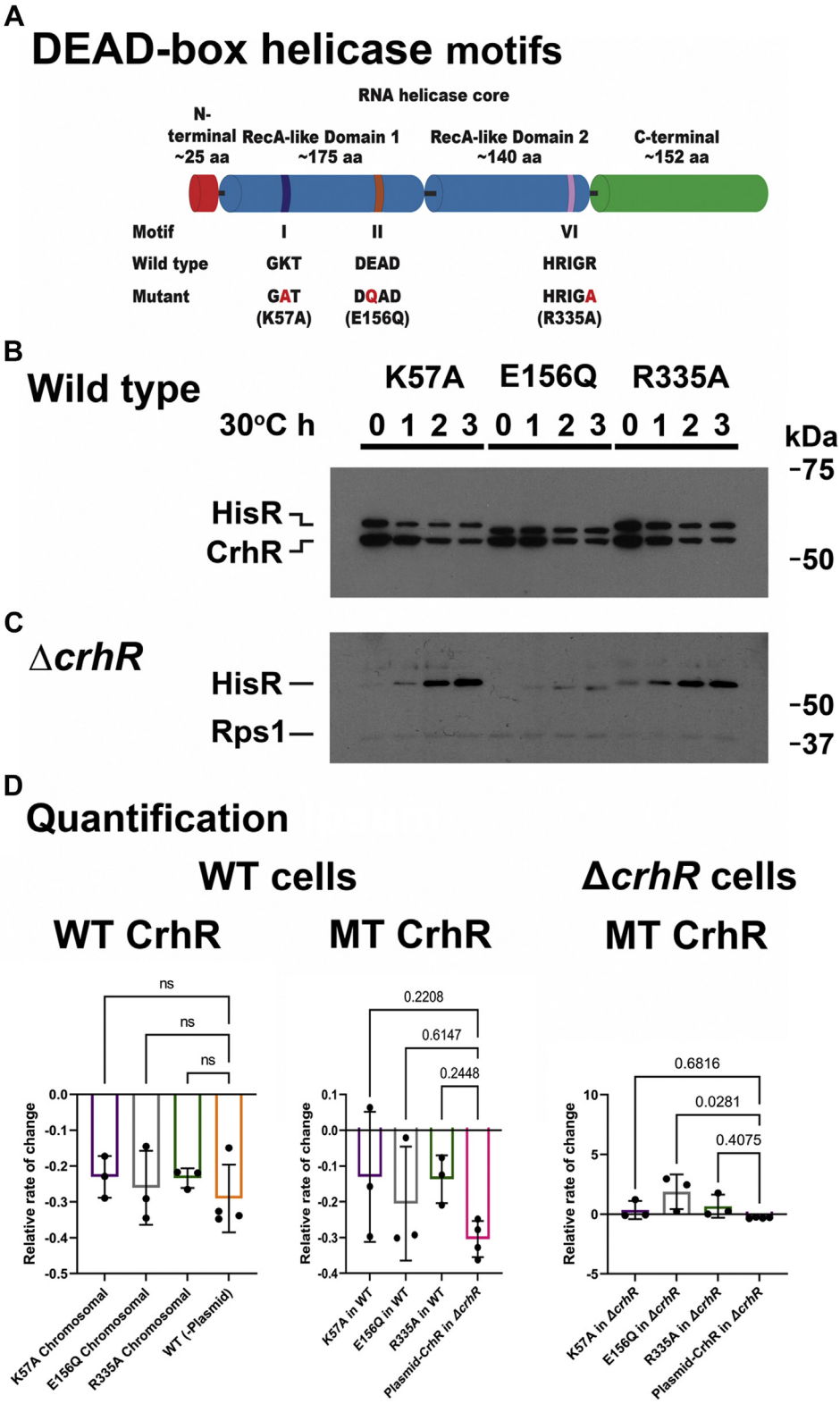

Figure 5. Biochemical inactivation of CrhR abolishes temperature regulation. *A*, location of the three point mutations used in the stability analysis, in relation to the helicase core and within defined motifs known to impact RNA helicase activity. Abundance of the 6X-His-tagged mutants, K57A (Walker box A, motif I), E156Q (DEAD box, motif II), or R335A (HRIGR box, motif VI), were assessed in WT (*B*) or Δ*crhR* (*C*) cells at the indicated times following maximal CrhR induction for 3 h at 20 °C (T = 0) and subsequent upshift to 30 °C. Lanes contain 10 μg of protein. CrhR and His-CrhR mutant abundance were detected by Western blotting and ECL detection and (*D*) the degradation rate of CrhR polypeptides quantified as described in Figure 2. CrhR, cyanobacterial RNA helicase redox.

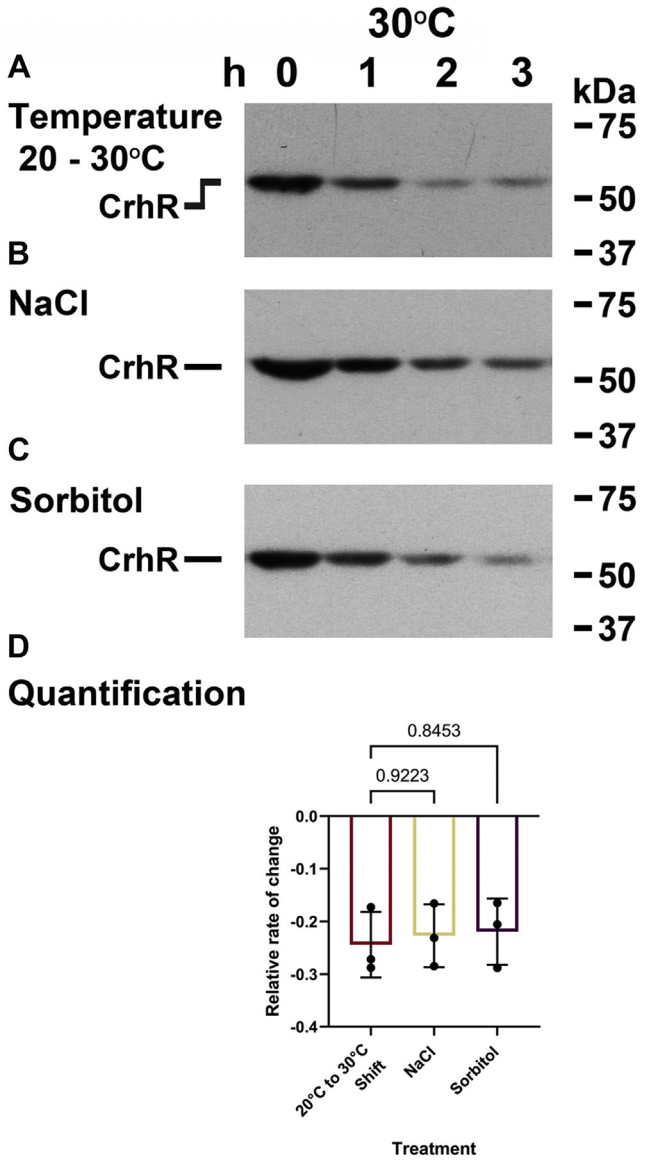

Figure 6. Removal of abiotic stress induces temperature-independent CrhR degradation. A WT *Synechocystis* culture was grown to mid-log phase at 30 °C before subjection to the following stresses at 30 °C for 3 h: *A*, temperature downshift (20 °C); *B*, NaCl (600 mM); *C*, sorbitol (600 mM). Induction under these conditions is shown as T = 0 30 °C. The stresses were removed by harvesting cells by vacuum filtration and suspension in fresh BG-11 at 30 °C, and cultures sampled each hour for 3 h at 30 °C. Lanes contain 15 μg of protein extract. Protein extracts were probed for CrhR abundance using Western blotting and ECL detection. *D*, quantification of the degradation rate of CrhR polypeptides, as described in Figure 2, using abundances observed immediately after stress removal normalized to 1.0 at T = 0. CrhR, cyanobacterial RNA helicase redox.

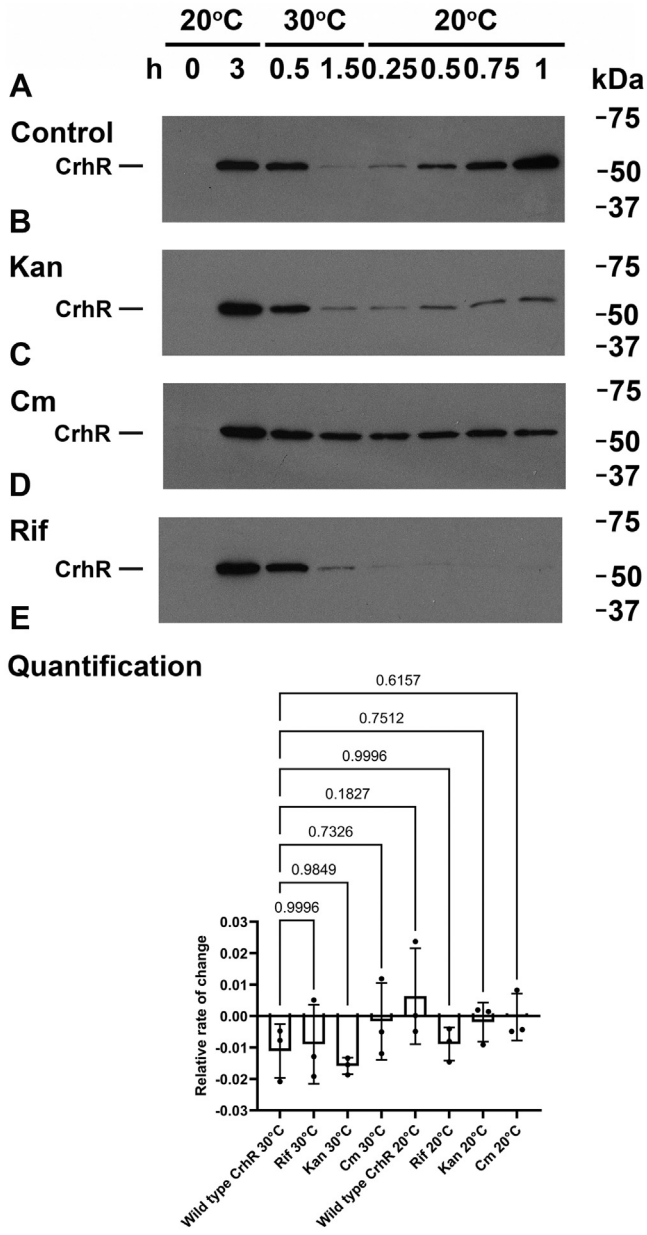

Figure 7. Translation inhibition effect on CrhR expression. *A*, a WT *Synechocystis* culture was grown to mid-log phase at 30 °C (20 °C T = 0) and induced for maximal CrhR induction by incubation at 20 °C for 3 h (20 °C T = 180). The culture was divided into four aliquots and incubated at 30 °C for 30 min prior to addition of nothing (*A*), kanamycin (*B*, 200 μg/ml), chloroamphenicol (*C*, 250 μg/ml), or rifampicin (*D*, 400 μg/ml). Incubation was continued at 30 °C for 1 h followed by transfer to 20 °C for 1 h. Lanes contain 15 μg of protein extract. CrhR protein was characterized by Western blotting and ECL detection. *E*, quantification. The degradation rates of CrhR polypeptide abundance were calculated to compare the relative rates of change between the 0.5 and 1.5 h time points at 30 °C and the relative rate at 20 °C over the four time points using the 30 °C 1.5 h abundance as 100%, as described as in Figure 2.

30 °C as evidenced by the growth defect in Δ*crhR* cells observed at 30 °C (45). Previous data have illustrated that a basal, low level of CrhR persisted at higher temperatures, indicating that proteolytic degradation is transient and not intended to completely eliminate CrhR (33). The kinetics of CrhR turnover have only been exhaustively characterized for the 20 to 30 °C transition. Here, aliquots of a 10 °C cold shocked culture were subjected to a time course analysis after temperature upshift directly to either 20 °C, 30 °C, or 40 °C to evaluate degradation dynamics (Fig. 8*A*). A shift from 10 to 20 °C did not elicit a significant proteolytic response (compare Fig. 8*A* 10 and 20 °C). Temperature upshift to 30 °C or 40 °C were significant enough, however, to elicit degradation of CrhR, suggesting that a threshold temperature exists between 20 °C and 30 °C that must be exceeded to elicit CrhR

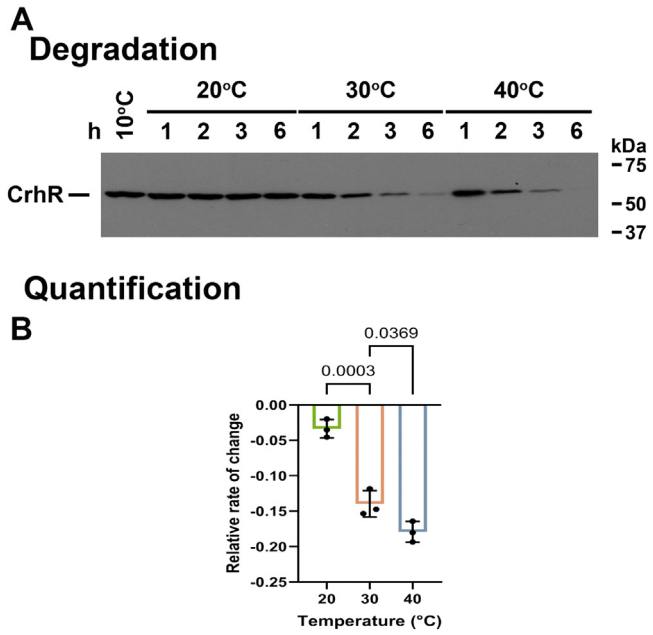

Figure 8. A threshold temperature triggers CrhR degradation. *A*, a WT *Synechocystis* culture was grown to mid-log phase at 30 °C prior to cold shock at 10 °C for 24 h. Aliquots were incubated at 20 °C, 30 °C, or 40 °C, and samples harvested as indicated. *B*, quantification. Levels of CrhR were standardized to the signal intensity at 10 °C using Image Studio Lite (LI-COR Biosciences). Lanes contain 15 μg of protein extract. CrhR protein was detected by Western blotting and ECL detection and the CrhR degradation rate quantified as described in Figure 2, including all time points. CrhR, cyanobacterial RNA helicase redox.

destabilization. Above this threshold, cells are sensitive to the degree of upshift, permitting establishment of a higher basal level of CrhR at 30 °C *versus* 40 °C (Fig. 8*A*). How this basal level is reached could be a product of either the amount of time proteolysis is active or differential magnitude of the degradation activity. Quantification of CrhR abundance for cells shifted from 10 to 20 °C reveals a modest rate of decline, while a 10 to 30 °C shift significantly enhances degradation (Fig. 8*B*). This rate was further stimulated in response to a 10 to 40 °C shift, resulting in the enhanced basal level observed at 30 °C *versus* 40 °C (Fig. 8*B*). Thus, the mechanism responsible for CrhR degradation must convey a detailed input regarding the magnitude of temperature upshift into an appropriate level of proteolytic activity to achieve the required CrhR abundance at each temperature.

AlphaFold predicts the CrhR CTE is a dimerization domain

To better understand the CTE of CrhR, the structure of residues 375 to 427 was predicted by the protein folding algorithm AlphaFold2 using the ColabFold implementation (46, 47). AlphaFold returned a dimeric model that consisted of two bundles of three helices each, that fold against each other (Fig. 9*A*). Side and top depictions of the model structure are shown in Figure 9, *A* and *B* with the interacting helices H1–H3 labeled from the N to C terminus.

AlphaFold predicts this model with high confidence by both predicted local-distance difference test (Fig. S2*A*) and the predicted alignment error (Fig. S2*B*). Indicating high local confidence around each amino acid and position/orientation confidence between the monomers, respectively (46, 48, 49). The model was also compared to known structures of DEAD-box helicase dimerization domains from cold-shock DEAD-box protein A (CsdA), cold shock helicase A, and heat resistant RNA-dependent ATPase (Fig. 9, *C* and *D*) (50–52). And, in spite of low sequence identity (Fig. S3), the model aligns well with an average RMSD of 3.8 Å (Fig. S2). To verify the prediction that CrhR is a homodimer, the oligomeric state in solution was determined by mass photometry. Mass photometry estimates molecular weights of proteins by detecting light scattering as single molecules interact with a glass coverslip. The intensity of the light scattering is compared to known molecular weight standards to obtain the estimates. Over time, a population is generated, and gaussian curves are fit to the population to identify individual species (53). The major species observed accounted for 93% of the protein in solution and had a MW of 107 kDa ± 15 kDa (Fig. 9*E*). This is within ∼9% error of the deduced dimer molecular weight (111.88 kDa) indicating that CrhR exists predominantly as a homodimer in solution.

Finer AlphaFold modeling of residues 215 to 445, corresponding to the second RecA domain (RecA2) and the entire CTE, was performed to predict the level of occlusion of the C-terminal degron sequence D412-W435. The degron is shown in red and is more solvent exposed than the subsequence Q417-Q425, shown in orange (Fig. 9*F*). However, despite extending past the end of H3, residues S431-W435 are predicted to pack against the RecA2 domain with an average predicted local-distance difference test score of 83.6 (Fig. S2, *C* and *D*). This tight packing would pose a steric hindrance for recognition of the degron.

Taken together, the AlphaFold predicted structure suggests that the CrhR C-terminal degron forms a three-helix bundle that homodimerizes to form a structure similar to the dimerization domains observed in the bacterial DEAD-box RNA helicases CsdA, cold shock helicase A, and Hera.

Discussion

Expression of CrhR, the sole DEAD-box RNA helicase encoded in the *Synechocystis* genome, is induced by a variety of abiotic stresses and repressed by proteolysis, a conditional mechanism induced by removal of the stress (32, 33, 44, 54). Proteolytic degradation represents a powerful yet flexible method for shaping the proteome in all cells, not just through routine protein turnover but also by way of targeted degradation influencing crucial cellular pathways. Through the remodeling of RNA secondary structure, RNA helicases act as important regulators of all aspects of RNA metabolism, impacting processes ranging from transcription to translation and degradation (37). Here we show *in vivo* that conditional degradation of CrhR requires an inherent 24 amino acid sequence, $CrhR_{D412\text{-}W435}$, located in a conserved 50 amino acid CrhR-specific motif, $CrhR_{K386\text{-}W435}$ within the CTE. AlphaFold structural analysis predicted that access and thus activity of this degron motif would be restricted by occlusion in a dimeric

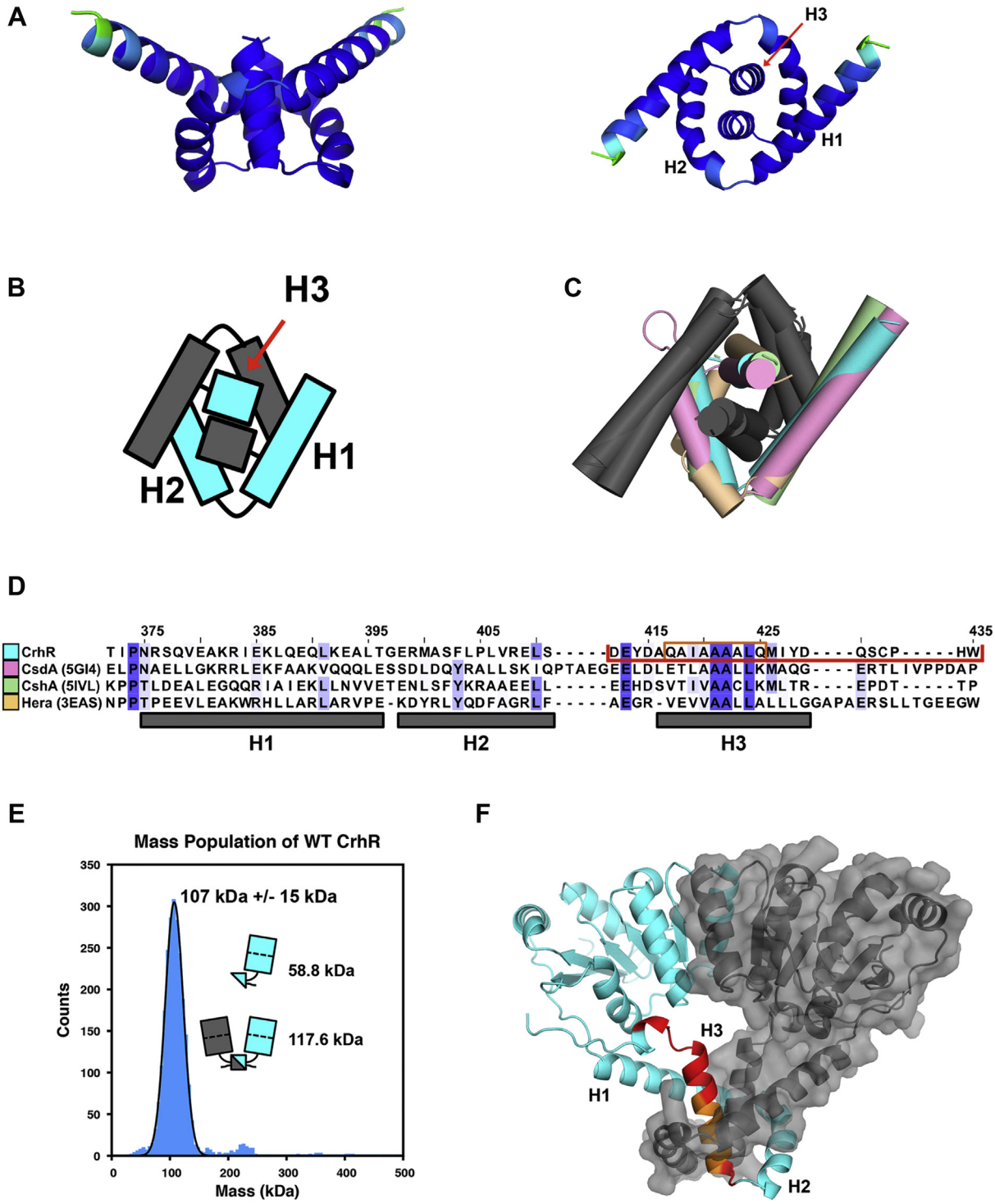

Figure 9. CrhR residues 375 to 427 are predicted to be responsible for CrhR homodimerization. *A*, side and top view of the AlphaFold model of CrhR residues 375 to 427. Residues are colored by predicted Local Distance Difference Test (pLDDT) score. pLDDT scores >90 (*dark blue*) indicate high confidence in both Cα and side chain position, while pLDDT scores between 70 and 90 (*green-cyan*) indicate high confidence in Cα position alone. *B*, *cartoon* depiction of a top view of the model. *C*, alignment of dimerization domains from CsdA (5GI4, *pink*), CshA (5IVL, *green*) and Hera (3EAS, *orange*) with the predicted AlphaFold structure of CrhR (*cyan*). *D*, sequence alignment of CrhR, CsdA, CshA, and Hera in the CTE region comprising the dimerization domain. *Blue highlights* indicate level of residue consensus. The region highlighted in *red* are residues D412-W435 which contains the entire degron while the subsequence of Q417-Q425 is highlighted in *orange*. *E*, mass photometric profiles obtained for 6xHis-CrhR. Theoretical MW for monomeric and dimeric species are shown. *F*, AlphaFold model of CrhR residues 215 to 445. Regions highlighted in *D* are colored on the *cyan* monomer. CrhR, cyanobacterial RNA helicase redox; CsdA, cold-shock DEAD-box protein A; CshA, cold shock helicase A; CTE, C-terminal extension; Hera, heat resistant RNA-dependent ATPase.

species. In addition, CrhR was required for the translation of an unknown degradation factor indicating that activity of the degradation machinery was autoregulatory. Thus, from an evolutionary perspective, the CrhR CTE is unique, encompassing the identified degron within a highly conserved 50 amino acid domain that defines a separate clade of DEAD-box RNA helicases found only in cyanobacteria (55).

CrhR degron structure

Using a phylogenetically guided deletion approach, we show that the CrhR degron is composed of an inherent, bipartite structure whose regions do not contribute equally to degradation. $CrhR_{K386\text{-}W411}$ appears to function in a supportive role, possibly as a regulatory or structural element while $CrhR_{D412\text{-}W435}$ contains the degron sequence. The presence of both domains was required for WT levels of degradation.

The dual CrhR degron therefore appears to function in a manner similar to the DnaA (14) and the SsrA (56) degrons, composed of functionally independent regions. Additional structure-function analysis, including fusion of the CrhR degron regions identified here to reporter genes, will be essential to further dissect the amino acid sequence participation in the proteolytic mechanism.

CrhR is a homodimer

AlphaFold *in silico* analysis predicted and mass photometry *in vitro* at 22 °C confirmed that CrhR is a homodimer. AlphaFold structural modeling also revealed significant structural similarities between the CrhR CTE motif, $CrhR_{K386\text{-}W435}$, and the CsdA dimerization domain (50). In CsdA, dimer stability is temperature dependent owing to differential activity of the CsdA dimerization domain, with stable associations observed at 24 °C that discourage monomer switching while incubation at 37 °C resulted in rapid monomer switching. The observed structural conservation between CsdA and CrhR is expected to be indicative of the functionality of the CrhR CTE motif as well and thereby suggests a regulatory mechanism by which the CrhR degron could be exposed and thus active under nonpermissive conditions. The dimer species was stable over all conditions assayed, but we predict that temperature upshift or salt concentration could result in protein unfolding, revealing the degron sequence to initiate degradation. Dimerization-mediated autoregulation of CrhR stability would constitute an additional level of control, allowing rapid fine-tuning of CrhR abundance and thus activity, enhancing cyanobacterial fitness in response to changing environmental conditions. However, these are predictions, and further study is required to elucidate the dynamics of CrhR structure under these conditions.

Conditional degradation of CrhR involves an autoregulatory mechanism

CrhR autoregulation of its own expression has previously been reported at a number of levels (32, 33, 36, 57). Here, we extend these observations by showing that autoregulation performs crucial roles in the degradation mechanism. Physiologically, alteration of CrhR degradation by both antibiotic inhibition and biochemical inactivation of helicase activity supports a scenario that implicates CrhR autoregulated translation of a factor required for degradation.

Biochemically, translation autoregulation may involve CrhR-mediated changes in gene expression initiated by RNA secondary structure rearrangements catalyzed by dsRNA unwinding, ssRNA annealing, and strand exchange (43). Related, it is also insightful that plasmid-based enhanced CrhR abundance proportionately decreased WT CrhR expression from the genome. Although the mechanism is unknown, it appears to involve an autoregulatory, negative feedback system and suggests that the cell can actively monitor levels of CrhR. This unexpected outcome further emphasizes that CrhR abundance is tightly regulated within an appropriate window as dictated by environmental conditions. These predictions were substantiated by the observation that CrhR interacts with the *crhR* transcript in pull-down experiments (36).

Indeed, similar autoregulatory loops mediate controlled degradation of transcription factors through their direct regulation of protease or adaptor abundance (58, 59). A pathway that resembles the proposed thermal-induced structural regulation of CrhR is observed for the DNA binding protein RovA that acts as a dimeric thermosensor to modulate virulence in *Yersinia pestis* (60). RovA functions as a transcription factor between 20 °C and 25 °C, enacting virulence programming necessary for host invasion and infection. A temperature increase to 37 °C, indicative of a mammalian host, causes a conformational shift that impairs RovA DNA binding and promotes proteolysis by Lon/Clp proteases. Dimerization of RovA monomers is achieved through extensive interactions between α helices, similar to the CsdA dimerization domain. While a number of thermosensing proteins have been described, the mechanisms generally do not involve degradation but are reversible and most frequently observed in pathogenic bacteria (61).

Role of temperature-regulated CrhR expression

Although their applicability to *Synechocystis* remains to be fully elucidated, insights from other model systems reveal that DEAD-box helicases are dynamic regulators that perform fundamental roles in assembly and/or activity of duplex RNA and/or RNP complexes thereby influencing all stages in the lifecycle of an RNA (37, 38, 62). In examining the physiological importance of CrhR, omics analysis has indicated that the absence of functional CrhR RNA helicase activity disrupts the expression of genes associated with photosynthetic and translation competency, particularly during cold stress, leading to a severe cold stress phenotype (34–36, 45). It is typically hypothesized that helicase resolution of thermally trapped RNA secondary structure is a prime mechanism regulating these influences on gene expression at low temperature (63). Such a role explains the necessity for CrhR induction, but not necessarily degradation. Clearly however, our data reveal that *Synechocystis* is highly sensitive to CrhR abundance, and modulation of genomic CrhR expression can occur in response to stable, persistent forms of CrhR.

Functionally, recent reports indicating that deletion of *crhR* decreased *clpP* and *clpR* transcript accumulation at 30 °C (35) combined with the co-immunoprecipitation of the protease transcript *ftsH2* with CrhR (36) potentially implicate these subunits as components of the proteolytic machinery. The known localization of CrhR and Clp/FtsH proteases on the thylakoid membrane could then catalyze degradation at the site of CrhR activity (39).

From an evolutionary perspective, the CrhR degron and the associated degradation machinery define a unique regulatory mechanism specific to cyanobacteria. Characterization of this inherent degron, controlling the autoregulatory proteolytic degradation of CrhR-like RNA helicases, identifies a novel mechanism of conditional proteolysis in bacteria. In addition, RNA helicase activity has not previously been implicated in proteolytic pathways, nor has degron-mediated degradation been identified as a regulator of DEAD-box RNA helicase abundance in other systems. In conjunction, and from an evolutionary perspective, low-resolution small angle X-ray scattering data have recently identified that the eukaryotic RNA helicase DDX21 contains an AAXL motif and displays dimerization in solution (64). Thus, similar domains exist in other Kingdoms and the potential for thermal regulation of oligomer state and polypeptide stability in these RNA helicases remain to be elucidated.

Since CrhR turnover exhibits considerable flexibility in both the environmental inducing signal and magnitude of the response, the CrhR degron represents a promising biotechnological module for fine-tuning heterologous protein stability in cyanobacteria containing CrhR-related proteins. Although our data connect temperature shift-induced changes in CrhR helicase abundance to the sequence and structure of the CTE, future work will be required to further clarify how the CrhR degron is connected to the physiological function of CrhR type helicases and why the intracellular concentration of these proteins is so tightly regulated.

Experimental procedures

Bacterial strains and culturing

Cyanobacterial and *E. coli* strains used in this study are listed in Table 1. The freshwater photoautotrophic cyanobacterial strains used in this study, *Synechocystis* sp. strain PCC 6803, *Nostoc* sp. strain PCC 7120, and *Leptolyngbya* sp. 696 were maintained on BG-11, while the marine *Synechococcus* sp. strain PCC 7002 was maintained on A+ medium supplemented with Vitamin B12 (65). A *Synechocystis* Δ*crhR* mutant in which the entire *crhR* ORF was replaced with a kanamycin resistance cassette was grown as described previously (33). Cells were grown in liquid BG-11 or A+ media at 30 °C with continuous shaking (150 rpm) coupled with bubbling with humidified air at an illumination of 50 μmol photons m^{-2} s^{-1}. Transformed *Synechocystis* cultures were supplemented with either gentamycin (10 μg/ml) or with a combination of gentamycin and kanamycin (50 μg/ml) for Δ*crhR* strains. Plasmids were propagated in either DH5α or XL-1 Blue strains of *E. coli* using gentamycin (10 μg/ml) supplemented Luria-Bertani broth.

crhR constructs

Plasmids and primers used in this study are listed in Table 1. A cold inducible plasmid construct was assembled using the pMON 36456 plasmid as a template (66). To remove the constitutive *nirA* promoter, pMON 36456 was digested with *Nde*I and *Stu*I, overhangs filled in with Klenow DNA pol and self-ligated to create ΔPpMON. A region containing the entire *crhR* ORF, including the native 5′ and 3′ UTRs, was cloned into ΔPpMON from cs0096-9 using *Eco*RI and *Xba*I to create ΔPpMON-CrhR (54). The 316 base pair operon promoter from upstream of *slr0082* was amplified using dcsr30f and dcsr30r (Table 1), digested with *Not*I and *Eco*RI and ligated into ΔPpMON-CrhR using the same restriction sites to create plasmid B1.

The B1 plasmid was used as a template to generate the N- and C-terminal *crhR* deletions by inverse PCR. For the N-terminal deletion, the initiator Met was left intact and T2-G26 were deleted, leaving a phenylalanine as the second amino acid that did not destabilize the mutant protein. For inactivation of RNA helicase core motifs, pMON-His-CrhR was used as a template in QuikChange PCR to introduce point mutations (33). Constructs were verified by sequencing prior to transformation of WT or Δ*crhR Synechocystis* by triparental mating.

Cyanobacterial triparental mating

Synechocystis cells were transformed by using a modified triparental mating protocol (67, 68). Plasmids were first transformed into *E. coli* DH5α carrying the helper plasmid pRL623 prior to transfer to *Synechocystis* using *E. coli* DH5α cells containing the conjugative plasmid RP4. The transformation mixture was spread on BG-11 agar plates supplemented with 5% LB and incubated under low light for 2 to 3 days. Bacteria were washed off these plates with BG-11 and spread on selective BG-11 plates supplemented with increasing gentamycin concentration (2, 5, and 10 μg/ml).

Bioinformatics analysis

Sequences of 22 cyanobacterial DEAD-box RNA helicases with homology to CrhR (Table S1) were identified by a BLASTp search of the NCBI nonredundant protein sequences database, restricted to cyanobacteria (taxid:1117), with *Synechocystis* CrhR (BAA10556.1) as the query sequence. These sequences were aligned in MEGA 7 (version 7.0.21) (69) using the MUSCLE algorithm (70) with default parameters. The 50 amino acid conserved motif was identified in the alignments using the MEME program (71) available in the MEME Suite (version 4.11.3) (72).

Time course evaluation of CrhR stability

To examine the degradation characteristics of CrhR mutants within *Synechocystis*, WT or Δ*crhR* transformants were grown at 30 °C to mid-log phase (A_{750} ∼ 0.4), transferred to

Table 1
Oligonucleotide, plasmid, and bacterial strain information

Strains, oligonucleotides, or plasmids utilized	Sequence or defining characteristic	Source, reference, or application
Cyanobacteria		
Synechocystis sp. PCC 6803	WT	(54)
Δ*crhR*	Replacement of the entire *crhR* ORF with a kanamycin resistance cassette	(33)
Nostoc sp. PCC 7120		Canadian Phycological Culture Collection
Leptolyngbya sp. 696		Canadian Phycological Culture Collection
Synechococcus sp. PCC 7002		Dr Donald Bryant
E. coli		
DH5α	Plasmid propagation	Laboratory collection
DH5α pRL623	Proper methylation of plasmid DNA prior to cyanobacterial transformation	Dr Jeff Elhai
DH5α RP4	Transfer of plasmid constructs to cyanobacteria	Dr Jeff Elhai
Plasmids		
pMON 36546	*E. coli* and *Synechocystis* shuttle vector, Gm^R	(65)
B1	pMON-*crhR* with the *slr0082* promoter	This study
B1-*crhR* ΔK449-Q492	C-terminal cutback, −45	This study
B1-*crhR* ΔE393-Q492	C-terminal cutback, −100	This study
B1-*crhR* ΔA347-Q492	C-terminal cutback, −147	This study
B1-*crhR* ΔR228-Q492	C-terminal cutback, −265	This study
B1-*crhR* ΔT2-G26	N-terminal cutback, ΔNTE	This study
B1-*crhR* ΔK386-S411	CrhR motif, ΔFront	This study
B1-*crhR* ΔD412-W435	CrhR motif, ΔBack	This study
B1-*crhR* ΔK386-W435	CrhR motif, ΔWhole	This study
B1-*crhR* ΔQ417-Q425	CrhR motif, ΔQ-Q	This study
pMON-His-CrhR	6His-*crhR* fusion in pMon 36546	(33)
pMON-His-K57A	pMON-His-CrhR point mutant	This study
pMON-His-E156Q	pMON-His-CrhR point mutant	This study
pMON-His-R335A	pMON-His-CrhR point mutant	This study
Oligonucleotides		
dcsr30f	ATATCCGCGGCCGCCCGGGAAAAG	Amplification of *slr0082* promoter
dcsr30r	CAGACCCTTTGAATTCGTAAAGACATTG	Amplification of *slr0082* promoter
DSW6	TAGTTCTAGATGATCAGGGC	Binds pMON 36546 backbone, used for all C-terminal cutbacks
DSW8	TTAGTTGAAATCAACTTCCG	B1-*crhR* ΔK449-Q492 generation
DSW4	ATTGTGTCTAGACTTACTTGAGTTGTTCGTGCAG	B1-*crhR* ΔE393-Q492 generation
DSW7	TTAGATCGCCTTACCAGTCTTAC	B1-*crhR* ΔA347-Q492 generation
DSW12	TAGCTCGAGTTAGGGCACGTGATAAAGC	B1-*crhR* ΔR228-Q492 generation
BW23	CATGGAAAAGTTAAATAATTTCG	B1-*crhR* ΔT2-G26 generation
BW24	TTTGAGGCTCCCACC	B1-*crhR* ΔT2-G26 generation
BW25	TTCAATCCGCTTGGCTTC	B1-*crhR* ΔK386-S411 generation, B1-*crhR* ΔK386-W435 generation
HG1	GATGAGTACGATGCCCAG	B1-*crhR* ΔK386-S411 generation
HG2	GCTCAATTCCCGCACTAAAGG	B1-*crhR* ΔD412-W435 generation
BW26	ATGAAATCCGATTGGGAAGTG	B1-*crhR* ΔD412-W435 generation, B1-*crhR* ΔK386-W435 generation
BW30	GGCATCGTACTCATCGC	B1-*crhR* ΔQ417-Q425 generation
BW31	ATGATCTATGACCAGAGCTG	B1-*crhR* ΔQ417-Q425 generation
DSW1	AAACCGGCACGGGGGCAACCGCCGCCTTTG	K57A FWD
DSW2	CAAAGGCGGCGGTTGCCCCCGTGCCGGTTT	K57A REV
GWO88	CAATGGGTGGTGCTGGATCAAGCGGACG AAATGCTGAGC	E156Q FWD
GWO89	GCTCAGCATTTCGTCCGCTTGATCCAGCA CCACCCATTG	E156Q REV
DSW13	CATTCACCGCATTGGCGCCACCGGTCGGG CTGG	R335A FWD
DSW14	CCAGCCCGACCGGTGGCGCCAATGCGGTG AATG	R335A REV

20 °C for 3 h to induce maximal CrhR accumulation and then returned to 30 °C to initiate CrhR degradation. For analysis of CrhR ortholog stability, *Synechocystis*, *Nostoc*, *Lyngbya*, and *Synechococcus* were grown to mid-log phase at 30 °C and transferred either to 20 °C for 3 h (*Synechocystis*, *Synechococcus*) or 10 °C for 24 h (*Nostoc*, *Lyngbya*) to induce helicase protein accumulation. Cultures were returned to 30 °C and sampled at the indicated times. Cells were harvested by centrifugation at the growth temperature, and cell pellets stored at −80 °C prior to Western blot analysis.

To assess the effect of a temperature gradient on CrhR degradation kinetics, a WT *Synechocystis* culture grown at 30 °C to mid-log phase was placed at 10 °C for 24 h. The culture was aliquoted, and the flasks transferred immediately to either 20 °C, 30 °C, or 40 °C for 6 h. Cells were collected by centrifugation at the indicated times at the stated growth temperature, and cell pellets were stored at −80 °C.

Influence of additional stresses on CrhR repression

Aliquots of a mid-log phase, WT *Synechocystis* culture grown at 30 °C were subjected to salt (600 mM) or sorbitol (600 mM) (38) stress in the absence of temperature stress at 30 °C for 3 h. A single aliquot was transferred to 20 °C to act as a control. Cells were collected on Durapore 0.22 μM GV membrane filters by vacuum using an EMD Millipore filter apparatus connected to a Trivac D4A pump. Cells were extensively washed with and suspended in fresh BG-11 media

and incubation continued at 30 °C for 3 h to observe CrhR degradation in the absence of stress.

Effect of translational and transcriptional inhibitors on CrhR degradation

Synechocystis WT cells were grown to mid-log phase at 30 °C and transferred to 20 °C for 3 h to induce maximal CrhR protein accumulation. Aliquots were transferred to 30 °C for 30 min, at which time chloramphenicol (250 μg/ml), kanamycin (200 μg/ml), rifampicin (400 μg/ml) or nothing (control) was added. Cultures were subsequently incubated for an additional hour at 30 °C prior to transfer to 20 °C for 1 h. Aliquots for protein isolation were harvested at the indicated times before and after either cold induction or antibiotic treatment, and the cell pellets were stored at −80 °C.

Protein extraction and western detection

Soluble protein extraction and western analysis were performed as described previously (32, 73). After Bradford standardization, aliquots of the clarified soluble fraction corresponding to the masses indicated were separated by SDS–10% PAGE and immunoblot detection of CrhR performed using anti-CrhR antisera (1:5000) and secondary antibody (anti-rabbit IgG at 1:20,000 dilution; Sigma-Aldrich) using enhanced chemiluminescence (ECL) (32). When indicated, Rps1 was used as a protein loading control. Representative data are shown from a minimum of three biological replicates.

Imaging of CrhR protein levels was conducted using either X-ray film (Fujifilm) or a ChemiDoc MP Imaging system (Bio-Rad). Quantification was performed using Image Studio Lite software (LI-COR), with Coomassie stained gels to correct for protein loading. A ratio representing the relative intensity of CrhR in each lane was obtained by dividing the corrected signal in that lane by the signal in the lane corresponding to the maximum induction, typically 3 h at 20 °C. Maximum induction required 24 h at 10 °C in the case of *Leptolyngbya* and *Nostoc*.

Statistical assessment of degradation

GraphPad Prism, version 9.1.1, for Windows (GraphPad Software) was used to visualize and then statistically analyze CrhR abundance data. Relative degradation rates were derived from averaging linear regression model slopes produced for all biological replicates from the corrected abundance values corresponding to the downregulation portion of each time course observed at 30 °C and using the level observed at 20 °C for 3 h or 24 h at 10 °C, as the maximum induction (T = 0 set to 1.0). Mean degradation rates were assessed for difference from the control condition using one-way ANOVA followed by a Dunnett's multiple comparisons test.

Protein structure modeling

CrhR structural modeling was performed using the ColabFold implementation of AlphaFold (https://github.com/sokrypton/ColabFold) (46, 47). The sequence of either residues 375 to 427 or 215 to 445 was input along with the input parameters listed in Table S2 into the AlphaFold2_MMseqs2 Google Colab notebook. Multiple sequence alignments were found using the MMseqs2 algorithm and were input along with the protein sequence to generate five models. The models were ranked by pTM score, and the highest scoring model was used for analysis.

Pymol (Version 2.4.0, Schrödinger, LLC) was used to compare known RNA helicase structures (PDB codes: 5IVL, 3EAS, 5GI4) with the AlphaFold models and for creating images. Confidence metrics were analyzed using python3 scripts and plotted with Gnuplot (Version 5.4, http://www.gnuplot.info/).

Model 375 to 427: This region was selected based on initial homology models to encompass the rigid core of the CTE. Colabfold, version 1.0, was used.

Model 215 to 445: This region was selected to encompass the environment around the CTE, through the relationships between the dimerization domain, the RecA2 domain, and the degron sequence. Colabfold, version 1.2, was used.

Purification of full-length CrhR

The *crhR* ORF cloned as a 6XHis tag in pRSET-A was overexpressed in BL21 DE3 cells using ampicilin (100 μg/ml) and 1 mM IPTG and grown for 18 h at 18 °C (43). The 2 l cell pellet was suspended in 100 ml of lysis buffer (50 mM Borate pH 9, 550 mM KCl, 1 mM EDTA, 1 mM DTT, cOmplete Protease Inhibitor Cocktail [Sigma-Aldrich Canada]) and disrupted by sonication and clarified by centrifugation. PEI (final concentration 0.5%) was added to the cleared lysate followed by centrifugation to remove DNA. The supernatant was subjected to a 60% ammonium sulphate precipitation followed by centrifugation. The pellets were suspended in a buffer consisting of 5 ml Hic A (50 mM Tris pH 8, 1 mM EDTA, 1 mM DTT) and 5 ml Hic B (50 mM Tris pH 8, 1.5 M ammonium sulphate, 1 mM EDTA, 1 mM DTT) and diluted to 135 ml with equal parts Hic A and Hic B. The protein was applied to a 25 ml butyl-sepharose reverse phase column (Amersham Biosciences, Inc). The column was washed with 20 ml of Hic B, and the protein eluted with a 100 ml linear gradient of Hic B to Hic A. CrhR containing fractions were pooled and diluted to 135 ml with a 2:1 ratio of Cat A buffer (50 mM Hepes pH 7.3, 1 mM EDTA, 1 mM DTT) and Cat B buffer (50 mM Hepes pH 7.3, 750 mM KCl, 1 mM EDTA, 1 mM DTT). Protein was loaded onto a 25 ml SP-Sepharose fast flow cation exchange column (Amersham Biosciences, Inc). The column was washed with 20 ml of Cat A, and the protein eluted with a 100 ml linear gradient from Cat A to Cat B. CrhR containing fractions were pooled and loaded onto a Superdex 200 16/60 size exclusion column (Amersham Biosciences, Inc) where the protein was eluted and stored in 10 mM Hepes pH 7.3, 500 mM KCl, 1 mM DTT.

Mass photometry

Commercial mass photometer (Refeyn Ltd) was used to determine the oligomeric state of purified 6xHis CrhR (53, 74). Protein (5.5 μM) in SEC buffer (10 mM Hepes pH 7.3, 500 mM

KCl, 1 mM DTT) was kept on ice, then diluted 90 times in the PBS buffer at 22 °C just before the experiment, and 15 μl of the mixture was placed on the well created by clean gaskets on top of clean microscope coverslip. Six thousand frames of data containing the contrast from different oligomeric state of the protein binding at the liquid glass interface were recorded by Refeyn Acquire^{MP} and analyzed by Discover^{MP} softwares. Mass of different oligomeric states of protein was determined from the calibration curve obtained from the known masses of BSA and Apoferritin. Data were plotted using a 5.2 kDa bin size in gnuplot. Gaussian curves were used to fit the data.

Data availability

All data described are included within the article or supporting information. All raw data from figures have been included as a single pdf file for reference.

Supporting information—This article contains supporting information (46, 48).

Acknowledgments—We wish to thank Reem Skeik and Dr Patrick Linder for advice during the initial CrhR dimerization experiments, Dr Jeff Elhai and Dr Donald Bryant for supplying *E. coli* and cyanobacterial strains, Dr Michael T. Woodside for use of equipment and Dr Paul Baumann for supplying the *E. coli* S1 antisera.

Author contributions—B. T. W., C. R. A. M., M. J. N. G., R. P. F., and G. W. O. conceptualization; B. T. W., C. R. A. M., D. S. W., S. S. P., and M. J. N. G. investigation; B. T. W., D. S. W., C. R. A. M., S. S. P., M. J. N. G., R. P. F., and G. W. O. formal analysis; B. T. W., C. R. A. M., M. J. N. G., R. P. F., and G. W. O. writing-original draft; B. T. W., D. S. W., C. R. A. M., S. S. P., M. J. N. G., R. P. F., and G. W. O. writing-review and editing.

Funding and additional information—This work was supported by the Natural Sciences and Engineering Research Council of Canada grant RGPIN-2016-05448 to G. W. O., 1705792 to R. P. F. and 2016–05163 to M. J. N. G.

Conflict of interest—The authors declare that they have no conflicts of interest with the contents of this article.

Abbreviations—The abbreviations used are: CrhR, cyanobacterial RNA helicase redox; CsdA, Cold-shock DEAD-box protein A; CTE, C-terminal extension; DEAD, Asp-Glu-Ala-Asp; NTE, N-terminal extension.

References

1. Gur, E., Biran, D., and Ron, E. Z. (2011) Regulated proteolysis in Gram-negative bacteria—how and when? *Nat. Rev. Microbiol.* **9**, 839
2. Jenal, U., and Hengge-Aronis, R. (2003) Regulation by proteolysis in bacterial cells. *Curr. Opin. Microbiol.* **6**, 163–172
3. Mahmoud, S. A., and Chien, P. (2018) Regulated proteolysis in bacteria. *Annu. Rev. Biochem.* **87**, 677–696
4. Dougan, D. A. (2013) *Regulated Proteolysis in Microorganisms*, Springer, Dordrecht, The Netherlands
5. Cohen, S. E., McKnight, B. M., and Golden, S. S. (2018) Roles for ClpXP in regulating the circadian clock in *Synechococcus elongatus*. *Proc. Natl. Acad. Sci. U. S. A.* **115**, E7805–E7813
6. Frees, D., Brøndsted, L., and Ingmer, H. (2013) Bacterial proteases and virulence. *Subcell. Biochem.* **66**, 161–192
7. Marr, A. K., Overhage, J., Bains, M., and Hancock, R. E. W. (2007) The Lon protease of *Pseudomonas aeruginosa* is induced by aminoglycosides and is involved in biofilm formation and motility. *Microbiology (Reading)* **153**, 474–482
8. Battesti, A., and Gottesman, S. (2013) Roles of adaptor proteins in regulation of bacterial proteolysis. *Curr. Opin. Microbiol.* **16**, 140–147
9. Varshavsky, A. (2011) The N-end rule pathway and regulation by proteolysis. *Protein Sci.* **20**, 1298–1345
10. Karzai, A. W., Roche, E. D., and Sauer, R. T. (2000) The SsrA–SmpB system for protein tagging, directed degradation and ribosome rescue. *Nat. Struct. Biol.* **7**, 449–455
11. Bittner, L. M., Westphal, K., and Narberhaus, F. (2015) Conditional proteolysis of the membrane protein YfgM by the FtsH protease depends on a novel N-terminal degron. *J. Biol. Chem.* **290**, 19367–19378
12. Hughes, A. C., Subramanian, S., Dann, C. E., 3rd, and Kearns, D. B. (2018) The C-terminal region of *Bacillus subtilis* SwrA is required for activity and adaptor-dependent LonA proteolysis. *J. Bacteriol.* **200**, e00659-17
13. Kihara, A., Akiyama, Y., and Ito, K. (1995) FtsH is required for proteolytic elimination of uncomplexed forms of SecY, an essential protein translocase subunit. *Proc. Natl. Acad. Sci. U. S. A.* **92**, 4532–4536
14. Liu, J., Zeinert, R., Francis, L., and Chien, P. (2019) Lon recognition of the replication initiator DnaA requires a bipartite degron. *Mol. Microbiol.* **111**, 176–186
15. Puri, N., and Karzai, A. W. (2017) HspQ functions as a unique specificity-enhancing factor for the AAA Lon protease. *Mol. Cell* **66**, 672–683
16. Langklotz, S., Schakermann, M., and Narberhaus, F. (2011) Control of lipopolysaccharide biosynthesis by FtsH-mediated proteolysis of LpxC is conserved in enterobacteria but not in all gram-negative bacteria. *J. Bacteriol.* **193**, 1090–1097
17. Pearce, M. J., Mintseris, J., Ferreyra, J., Gygi, S. P., and Darwin, K. H. (2008) Ubiquitin-like protein involved in the proteasome pathway of *Mycobacterium tuberculosis*. *Science* **322**, 1104–1107
18. Trentini, D. B., Suskiewicz, M. J., Heuck, A., Kurzbauer, R., Deszcz, L., Mechtler, K., and Clausen, T. (2016) Arginine phosphorylation marks proteins for degradation by a Clp protease. *Nature* **539**, 48–53
19. Knipfer, N., Seth, A., Roudiak, S. G., and Shrader, T. E. (1999) Species variation in ATP-dependent protein degradation: Protease profiles differ between mycobacteria and protease functions differ between *Mycobacterium smegmatis* and *Escherichia coli*. *Gene* **231**, 95–104
20. Liao, J.-Y. R., and van Wijk, K. J. (2019) Discovery of AAA protease substrates through trapping approaches. *Trends Biochem. Sci.* **44**, 528–545
21. Stein, B. J., Grant, R. A., Sauer, R. T., and Baker, T. A. (2016) Structural basis of an N-degron adaptor with more stringent specificity. *Structure* **24**, 232–242
22. Ishii, Y., and Amano, F. (2001) Regulation of SulA cleavage by Lon protease by the C-terminal amino acid of SulA, histidine. *Biochem. J.* **358**, 473–480
23. Shah, I. M., and Wolf, R. E., Jr. (2006) Sequence requirements for Lon-dependent degradation of the *Escherichia coli* transcription activator SoxS: Identification of the SoxS residues critical to proteolysis and specific inhibition of *in vitro* degradation by a peptide comprised of the N-terminal 21 amino acid residues. *J. Mol. Biol.* **357**, 718–731
24. Savakis, P., and Hellingwerf, K. J. (2015) Engineering cyanobacteria for direct biofuel production from CO_2. *Curr. Opin. Biotechnol.* **33**, 8–14
25. Soo, R. M., Hemp, J., Parks, D. H., Fischer, W. W., and Hugenholtz, P. (2017) On the origins of oxygenic photosynthesis and aerobic respiration in Cyanobacteria. *Science* **355**, 1436–1440
26. Jin, H., Kim, R., and Bhaya, D. (2021) Deciphering proteolysis pathways for the error-prone DNA polymerase in Cyanobacteria. *Environ. Microbiol.* **23**, 559–571
27. Tryggvesson, A., Ståhlberg, F. M., Töpel, M., Tanabe, N., Mogk, A., and Clarke, A. K. (2015) Characterization of ClpS2, an essential adaptor protein for the cyanobacterium *Synechococcus elongatus*. *FEBS Lett.* **589**, 4039–4046
28. Karradt, A., Sobanski, J., Mattow, J., Lockau, W., and Baier, K. (2008) NblA, a key protein of phycobilisome degradation, interacts with ClpC, a

HSP100 chaperone partner of a cyanobacterial Clp protease. *J. Biol. Chem.* **283**, 32394–32403
29. Nguyen, A. Y., Bricker, W. P., Zhang, H., Weisz, D. A., Gross, M. L., and Pakrasi, H. B. (2017) The proteolysis adaptor, NblA, binds to the N-terminus of β-phycocyanin: Implications for the mechanism of phycobilisome degradation. *Photosynth. Res.* **132**, 95–106
30. Khusnutdinova, A. N., Correia, K., Diep, P., Batyrovaa, K. A., Nemr, K., Flick, R., Stogios, P., Yakunin, A. F., and Mahadevan, R. (2020) A novel C-terminal degron identified in bacterial aldehyde decarbonylases using directed evolution. *Biotechnol. Biofuels* **13**, 114
31. Sokolenko, A., Pojidaeva, E., Zinchenko, V., Panichkin, V., Glaser, V. M., Herrmann, R. G., and Shestakov, S. V. (2002) The gene complement for proteolysis in the cyanobacterium *Synechocystis* sp. PCC 6803 and *Arabidopsis thaliana* chloroplasts. *Curr. Genet.* **41**, 291–310
32. Rosana, A. R. R., Chamot, D., and Owttrim, G. W. (2012) Autoregulation of RNA helicase expression in response to temperature stress in *Synechocystis* sp. PCC 6803. *PLoS One* **7**, e48683
33. Tarassova, O. S., Chamot, D., and Owttrim, G. W. (2014) Conditional, temperature-induced proteolytic regulation of cyanobacterial RNA helicase expression. *J. Bacteriol.* **196**, 1560–1568
34. Rowland, J. G., Simon, W. J., Prakash, J. S. S., and Slabas, A. R. (2011) Proteomics reveals a role for the RNA helicase crhR in the modulation of multiple metabolic pathways during cold acclimation of *Synechocystis* sp. PCC6803. *J. Proteome Res.* **10**, 3674–3689
35. Georg, J., Rosana, A. R. R., Chamot, D., Migur, A., Hess, W. R., and Owttrim, G. W. (2019) Inactivation of the RNA helicase CrhR impacts a specific subset of the transcriptome in the cyanobacterium *Synechocystis* sp. PCC 6803. *RNA Biol.* **16**, 1205–1214
36. Migur, A., Heyl, F., Fuss, J., Srikumar, A., Huettel, B., Steglich, C., Prakash, J. S. S., Reinhardt, R., Backofen, R., Owttrim, G. W., and Hess, W. R. (2021) The temperature-regulated DEAD-box RNA helicase CrhR interactome: Autoregulation and photosynthesis-related transcripts. *J. Exp. Bot.* **72**, 7564–7579
37. Linder, P., and Jankowsky, E. (2011) From unwinding to clamping - the DEAD box RNA helicase family. *Nat. Rev. Mol. Cell Biol.* **12**, 505–516
38. Redder, P., Hausmann, S., Khemici, V., Yasrebi, H., and Linder, P. (2015) Bacterial versatility requires DEAD-box RNA helicases. *FEMS Microbiol. Rev.* **39**, 392–412
39. Rosana, A. R., Whitford, D. S., Fahlman, R. P., and Owttrim, G. W. (2016) Cyanobacterial RNA helicase CrhR localizes to the thylakoid membrane region and cosediments with degradosome and polysome complexes in *Synechocystis* sp. strain PCC 6803. *J. Bacteriol.* **198**, 2089–2099
40. Rozen, F., Pelletier, J., Trachsel, H., and Sonenberg, N. (1989) A lysine substitution in the ATP-binding site of eucaryotic initiation factor 4A abrogates nucleotide-binding activity. *Mol. Cell. Biol.* **9**, 4061
41. Pause, A., Méthot, N., Svitkin, Y., Merrick, W. C., and Sonenberg, N. (1994) Dominant negative mutants of mammalian translation initiation factor eIF-4A define a critical role for eIF-4F in cap-dependent and cap-independent initiation of translation. *EMBO J.* **13**, 1205–1215
42. Pause, A., Methot, N., and Sonenberg, N. (1993) The HRIGRXXR region of the DEAD box RNA helicase eukaryotic translation initiation factor 4A is required for RNA binding and ATP hydrolysis. *Mol. Cell. Biol.* **13**, 6789–6798
43. Chamot, D., Colvin, K. R., Kujat-Choy, S. L., and Owttrim, G. W. (2005) RNA structural rearrangement via unwinding and annealing by the cyanobacterial RNA helicase, CrhR. *J. Biol. Chem.* **280**, 2036–2044
44. Ritter, S. P. A., Lewis, A. C., Vincent, S. L., Lo, L. L., Cunha, A. P. A., Chamot, D., Ensminger, I., Espie, G. S., and Owttrim, G. W. (2020) Evidence for convergent sensing of multiple abiotic stresses in cyanobacteria. *Biochim. Biophys. Acta Gen. Subj.* **1864**, 129462
45. Rosana, A. R. R., Ventakesh, M., Chamot, D., Patterson-Fortin, L. M., Tarassova, O., Espie, G. S., and Owttrim, G. W. (2012) Inactivation of a low temperature-induced RNA helicase in *Synechocystis* sp. PCC 6803: Physiological and morphological consequences. *Plant Cell Physiol.* **53**, 646–658
46. Jumper, J., Evans, R., Pritzel, A., Green, T., Figurnov, M., Ronneberger, O., Tunyasuvunakool, K., Bates, R., Žídek, A., Potapenko, A., Bridgland, A., Meyer, C., Kohl, S. A. A., Ballard, A. J., Cowie, A., *et al.* (2021) Highly accurate protein structure prediction with AlphaFold. *Nature* **596**, 583–589
47. [preprint] Mirdita, M., Ovchinnikov, S., and Steinegger, M. (2021) ColabFold - making protein folding accessible to all. *bioRxiv*. https://doi.org/10.1101/2021.08.15.456425
48. Tunyasuvunakool, K., Adler, J., Wu, Z., Green, T., Zielinski, M., Žídek, A., Bridgland, A., Cowie, A., Meyer, C., Laydon, A., Velankar, S., Kleywegt, G. J., Bateman, A., Evans, R., Pritzel, A., *et al.* (2021) Highly accurate protein structure prediction for the human proteome. *Nature* **596**, 590–596
49. Mariani, V., Biasini, M., Barbato, A., and Schwede, T. (2013) lDDT: A local superposition-free score for comparing protein structures and models using distance difference tests. *Bioinformatics* **29**, 2722–2728
50. Xu, L., Wang, L., Peng, J., Li, F., Wu, L., Zhang, B., Lv, M., Zhang, J., Gong, Q., and Zhang, R. (2017) Insights into the structure of dimeric RNA helicase CsdA and indispensable role of its C-Terminal regions. *Structure* **25**, 1795–1808
51. Huen, J., Lin, C.-L., Golzarroshan, B., Yi, W.-L., Yang, W.-Z., and Yuan, H. S. (2017) Structural insights into a unique dimeric DEAD-box helicase CshA that promotes RNA decay. *Structure* **25**, 469–481
52. Klostermeier, D., and Rudolph, M. G. (2009) A novel dimerization motif in the C-terminal domain of the *Thermus thermophilus* DEAD box helicase Hera confers substantial flexibility. *Nucleic Acids Res.* **37**, 421–430
53. Young, G., Hundt, N., Cole, D., Fineberg, A., Andrecka, J., Tyler, A., Olerinyova, A., Ansari, A., Marklund, E. G., Collier, M. P., Chandler, S. A., Tkachenko, O., Allen, J., Crispin, M., Billington, N., *et al.* (2018) Quantitative mass imaging of single biological macromolecules. *Science* **360**, 423–427
54. Kujat, S. L., and Owttrim, G. W. (2000) Redox-regulated RNA helicase expression. *Plant Physiol.* **124**, 703–714
55. Whitford, D. S., Whitman, B. T., and Owttrim, G. W. (2021) Genera specific distribution of DEAD-box RNA helicases in cyanobacteria. *Microb. Genom.* **7**, mgen000517
56. Flynn, J. M., Levchenko, I., Seidel, M., Wickner, S. H., Sauer, R. T., and Baker, T. A. (2001) Overlapping recognition determinants within the ssrA degradation tag allow modulation of proteolysis. *Proc. Natl. Acad. Sci. U. S. A.* **98**, 10584–10589
57. Albert, X., Rosana, R. R., Whitford, D. S., Migur, A., Steglich, C., Kujat-Choy, S. L., Hess, W. R., George, X., and Owttrim, W. (2020) RNA helicase-regulated processing of the *Synechocystis rimO-crhR* operon results in differential cistron expression and accumulation of two sRNAs. *J. Biol. Chem.* **295**, 6372–6386
58. Engman, J., Rogstam, A., Frees, D., Ingmer, H., and von Wachenfeldt, C. (2012) The YjbH adaptor protein enhances proteolysis of the transcriptional regulator Spx in *Staphylococcus aureus*. *J. Bacteriol.* **194**, 1186–1194
59. Iniesta, A. A., and Shapiro, L. (2008) A bacterial control circuit integrates polar localization and proteolysis of key regulatory proteins with a phospho-signaling cascade. *Proc. Natl. Acad. Sci. U. S. A.* **105**, 16602–16607
60. Herbst, K., Bujara, M., Heroven, A. K., Opitz, W., Weichert, M., Zimmermann, A., and Dersch, P. (2009) Intrinsic thermal sensing controls proteolysis of *Yersinia* virulence regulator RovA. *PLoS Pathog.* **5**, e1000435
61. Klinkert, B., and Narberhaus, F. (2009) Microbial thermosensors. *Cell. Mol. Life Sci.* **66**, 2661–2676
62. Sloan, K. E., and Bohnsack, M. T. (2018) Unravelling the mechanisms of RNA helicase regulation. *Trends Biochem. Sci.* **43**, 237–250
63. Iost, I., Bizebard, T., and Dreyfus, M. (2013) Functions of DEAD-box proteins in bacteria: Current knowledge and pending questions. *Biochim. Biophys. Acta* **1829**, 866–877
64. Marcaida, M. J., Kauzlaric, A., Duperrex, A., Sülzle, J., Moncrieffe, M. C., Adebajo, D., Manley, S., Trono, D., and Dal Peraro, M. (2020) The human RNA helicase DDX21 presents a dimerization interface necessary for helicase activity. *iScience* **23**, 101811
65. Mloszewska, A. M., Cole, D. B., Planavsky, N. J., Kappler, A., Whitford, D. S., Owttrim, G. W., and Konhauser, K. O. (2018) UV radiation limited

the expansion of cyanobacteria in early marine photic environments. *Nat. Commun.* **9**, 1–8
66. Qi, Q., Hao, M., Ng, W. O., Slater, S. C., Baszis, S. R., Weiss, J. D., and Valentin, H. E. (2005) Application of the *Synechococcus* nirA promoter to establish an inducible expression system for engineering the *Synechocystis* tocopherol pathway. *Appl. Environ. Microbiol.* **71**, 5678–5684
67. Elhai, J., and Wolk, C. P. (1988) Conjugal transfer of DNA to cyanobacteria. *Methods Enzymol.* **167**, 747–754
68. Elhai, J., Vepritskiy, A., Muro-Pastor, A. M., Flores, E., and Wolk, C. P. (1997) Reduction of conjugal transfer efficiency by three restriction activities of *Anabaena* sp. strain PCC 7120. *J. Bacteriol.* **179**, 1998–2005
69. Kumar, S., Stecher, G., and Tamura, K. (2016) MEGA7: Molecular evolutionary genetics analysis version 7.0 for bigger datasets. *Mol. Biol. Evol.* **33**, 1870–1874
70. Edgar, R. C. (2004) MUSCLE: Multiple sequence alignment with high accuracy and high throughput. *Nucleic Acids Res.* **32**, 1792–1797
71. Bailey, T. L., and Elkan, C. (1994) Fitting a mixture model by expectation maximization to discover motifs in biopolymers. *Proc. Int. Conf. Intell. Syst. Mol. Biol.* **2**, 28–36
72. Bailey, T. L., Boden, M., Buske, F. A., Frith, M., Grant, C. E., Clementi, L., Ren, J., Li, W. W., and Noble, W. S. (2009) MEME SUITE: Tools for motif discovery and searching. *Nucleic Acids Res.* **37**, W202–W208
73. Owttrim, G. W. (2012) RNA helicases in cyanobacteria: Biochemical and molecular approaches. *Methods Enzymol.* **511**, 385–403
74. Sonn-Segev, A., Belacic, K., Bodrug, T., Young, G., VanderLinden, R. T., Schulman, B. A., Schimpf, J., Friedrich, T., Dip, P. V., Schwartz, T. U., Bauer, B., Peters, J. M., Struwe, W. B., Benesch, J. L. P., Brown, N. G., *et al.* (2020) Quantifying the heterogeneity of macromolecular machines by mass photometry. *Nat. Commun.* **11**, 1–10